Cerebral Cortex January 2014;24:81–97
doi:10.1093/cercor/bhs287
Advance Access publication October 4, 2012

Temporal Coupling with Cortex Distinguishes Spontaneous Neuronal Activities in Identified Basal Ganglia-Recipient and Cerebellar-Recipient Zones of the Motor Thalamus

Kouichi C. Nakamura, Andrew Sharott and Peter J. Magill

Medical Research Council Anatomical Neuropharmacology Unit, Department of Pharmacology, University of Oxford, Oxford OX1 3TH, UK

Address correspondence to Dr Peter J. Magill, Medical Research Council Anatomical Neuropharmacology Unit, University of Oxford, Mansfield Road, Oxford OX1 3TH, UK. Email: peter.magill@pharm.ox.ac.uk.

Neurons of the motor thalamus mediate basal ganglia and cerebellar influences on cortical activity. To elucidate the net result of γ-aminobutyric acid-releasing or glutamatergic bombardment of the motor thalamus by basal ganglia or cerebellar afferents, respectively, we recorded the spontaneous activities of thalamocortical neurons in distinct identified "input zones" in anesthetized rats during defined cortical activity states. Unexpectedly, the mean rates and brain state dependencies of the firing of neurons in basal ganglia-recipient zone (BZ) and cerebellar-recipient zone (CZ) were matched during slow-wave activity (SWA) and cortical activation. However, neurons were distinguished during SWA by their firing regularities, low-threshold spike bursts and, more strikingly, by the temporal coupling of their activities to ongoing cortical oscillations. The firing of neurons across the BZ was stronger and more precisely phase-locked to cortical slow (~1 Hz) oscillations, although both neuron groups preferentially fired at the same phase. In contrast, neurons in BZ and CZ fired at different phases of cortical spindles (7–12 Hz), but with similar strengths of coupled firing. Thus, firing rates do not reflect the predicted inhibitory–excitatory imbalance across the motor thalamus, and input zone-specific temporal coding through oscillatory synchronization with the cortex could partly mediate the different roles of basal ganglia and cerebellum in behavior.

Keywords: basal ganglia, cerebellar nuclei, oscillation, spindle, thalamocortical

Introduction

The basal ganglia and cerebellum play vital and distinct roles in controlling voluntary movement. The so-called "motor thalamus" is a key substrate through which both basal ganglia and cerebellum influence neocortical activity (Jones 2007). Defining how these 2 largely nonoverlapping subcortical afferents (Groenewegen and Witter 2004) impact on motor thalamic activity in vivo is thus fundamentally important for understanding the neural basis of purposeful action (Nambu 2008). This issue extends to the spontaneous thalamic activities present "at rest", not least because they provide a baseline to interpret all movement-related neuronal firing. During quiet wakefulness, sleep, or anesthesia, γ-aminobutyric acid (GABA)-releasing neurons of basal ganglia output nuclei and presumed glutamatergic neurons of cerebellar nuclei often fire continuously at >25 spikes/s (Thach 1968; DeLong 1971; DeLong et al. 1983; Chiken and Tokuno 2003; Magill et al. 2004; Rowland and Jaeger 2005). How these highly active and neurochemically distinct inputs influence the spontaneous firing of their respective thalamic targets is unclear, particularly in relation to ongoing activity in the neocortex that aids definition of brain state. This is critical to consider because the firing mode of thalamocortical neurons, that is, the "bursting" or "tonic" activity favored by membrane hyperpolarization and depolarization, respectively, varies with brain state and behavior (Swadlow and Gusev 2001; Llinás and Steriade 2006).

Neurons of the basal ganglia output nuclei and cerebellar nuclei establish characteristically large axon terminals in the motor thalamus, which are assumed to support powerful, efficient synaptic transmission (Aumann et al. 1994; Sherman and Guillery 2006; Bodor et al. 2008). Because thalamic neurons in areas innervated by basal ganglia or cerebellar nuclei are under vigorous GABAergic (inhibitory) or glutamatergic (excitatory) bombardment, respectively, they should be readily distinguished by their spontaneous firing rates and patterns. Some electrophysiological recordings in motor thalamic nuclei, defined by cytoarchitecture or indirect mapping, in awake monkeys partly support this prediction (Vitek et al. 1994), but others do not (Anderson and Turner 1991). Relating the spontaneous activities of motor thalamic neurons to well-defined brain states could help resolve this discrepancy, as could recording identified neurons in motor thalamic areas delineated by their inputs rather than ambiguous cytoarchitectonics (Percheron et al. 1996). The importance of the latter is exemplified in rats; the territories ("zones") receiving inputs from basal ganglia and cerebellar nuclei do not tally well with traditional borders of the ventral anterior (VA), ventral lateral (VL), and ventral medial (VM) nuclei that constitute the motor thalamus (Sakai and Grofovà 2003; Groenewegen and Witter 2004; Kuramoto et al. 2011). Moreover, defining temporal activity dynamics beyond mean firing rate, for example, oscillatory synchronization, is a key to understanding the impact of different subcortical inputs on spontaneous thalamic activity, as established for functionally related somatosensory thalamic nuclei (Slézia et al. 2011). Because thalamocortical neurons in "basal ganglia-recipient zone" (BZ) and "cerebellar-recipient zone" (CZ) preferentially innervate layers 1 and 3–5, respectively, of wide frontal cortical areas (Herkenham 1979; Kuramoto et al. 2009, 2011; Rubio-Garrido et al. 2009), accounting for their potential phase-locking to cortical oscillations is crucial for understanding the interplay of basal ganglia and cerebellar circuits with cortical networks. To address these issues, we recorded motor thalamic neurons that were precisely localized to either BZ or CZ, identified by complementary distributions of GABAergic and glutamatergic axon terminal markers. Using analytical frameworks that considered both firing rate and pattern, we then characterized and compared spontaneous activities across a range of brain states.

Materials and Methods

Experimental procedures were performed on adult male Sprague Dawley rats (Charles River) and were conducted in accordance with the Animals (Scientific Procedures) Act, 1986 (United Kingdom).

Electrophysiological Recordings

Recordings were made in 38 rats (300–460 g). Anesthesia was induced with 4% v/v isoflurane (Isoflo, Schering-Plough) in O_2 and maintained with urethane (1.3 g/kg, intraperitoneal [i.p.] ethyl carbamate, Sigma), and supplemental doses of ketamine (30 mg/kg, i.p.; Willows Francis) and xylazine (3 mg/kg, i.p.; Bayer), as described previously (Magill et al. 2001). All wound margins were infiltrated with the local anesthetic bupivacaine (0.25% w/v; Astra), and corneal dehydration was prevented with application of Hypromellose eye drops (Norton Pharmaceuticals). Animals were then placed in a stereotaxic frame (David Kopf Instruments). Body temperature was maintained at 37 ± 0.5 °C using a homeothermic heating device (Harvard Apparatus). An electrocorticogram (ECoG), electrocardiographic activity, and respiration rate were monitored constantly to ensure the animals' well-being (Mallet et al. 2008). The ECoG was recorded via a 1-mm diameter steel screw juxtaposed to the dura mater above the right motor cortex (anteroposterior +4.2 mm, mediolateral: 2.0 mm in relation to Bregma; Paxinos and Watson 2007) and was referenced against another screw implanted in the skull above the cerebellum. These stereotaxic coordinates correspond to the medial agranular field of the motor cortex (Donoghue and Wise 1982; Brecht et al. 2004), which both projects to and receives input from the BZ and CZ of the rat motor thalamus (Herkenham 1979; Kincaid and Wilson 1996; Kuramoto et al. 2009). Raw ECoG was bandpass filtered (0.3–1500 Hz, −3 dB limits) and amplified (×2000, DPA-2FS filter/amplifier; Scientifica) before acquisition. A discrete craniotomy (~4 mm^2) was performed above the right thalamus, and the dura mater removed for the insertion of recording electrodes. Saline solution (0.9% w/v NaCl) was applied to all areas of the exposed cortex to prevent dehydration. Extracellular recordings of the action potentials ("spikes") of single motor thalamic neurons were made using 10–25 MΩ (measured in situ) glass electrodes (tip diameter 1.0–2.0 μm), which contained 0.5 M NaCl and Neurobiotin (1.5% w/v; Vector Laboratories). Electrodes were lowered into the brain under stereotaxic guidance and using a computer-controlled stepper motor (IVM-1000; Scientifica) that allowed the electrode depth to be determined with a resolution of 0.1 μm. Electrode signals were amplified (×10) through the active bridge circuitry of an Axoprobe-1A amplifier (Molecular Devices Corp.), coupled to alternating current, and further amplified (×100) and bandpass filtered (300–5000 Hz) to extract unit activity (DPA-2FS; Scientifica). A Humbug (Quest Scientific) was used in place of a traditional "notch" filter to eliminate mains noise at 50 Hz (Mallet et al. 2008). The action potentials of single units were often several mV in amplitude.

Assessment of Brain States

Thalamic neuron firing was recorded during 2 distinct, spontaneous brain states, as defined by the ECoG: 1) slow-wave activity (SWA; Fig. 1*D*,*H*), which is similar to activity observed during natural non-rapid eye movement sleep and drowsiness; and 2) "cortical activation" (Fig. 1*E*,*I*), which contains patterns of activity that are more analogous to those observed during the alert, behaving state (Steriade 2000). In frontal ECoGs, the former state is characterized by a slow (~1 Hz) oscillation of large amplitude (>400 μV). In this recording configuration, cortical neurons are only active during the surface-positive component of the slow oscillation. Higher-frequency activity of smaller amplitude (<200 μV), including spindle oscillations (7–12 Hz), was often superimposed on specific portions of the slow oscillation, both of which are the hallmarks of SWA in general (Magill et al. 2000; Steriade 2000, 2006). In contrast, the latter activated brain state contained patterns of low-amplitude (<100 μV) cortical activity that are qualitatively analogous to those observed during wakefulness (Steriade 2000). Transition from SWA to the activated brain state is exemplified by obliteration of cortical slow (~1 Hz), delta (2–4 Hz) and spindle (7–12 Hz) oscillations (Steriade 2000). Notably, the neuronal activity patterns present under this anesthetic regimen may only be qualitatively similar to those present in the unanesthetized brain (Chauvette et al. 2011). Nevertheless, the urethane-anesthetized animal serves as a useful model for assessing the impact of extremes of brain state on functional connectivity within and between the thalamus, cortex, and basal ganglia (Magill et al. 2006; Steriade 2000, 2006). Cortical activation was occasionally elicited by pinching the hindpaw for 10–15 s with serrated forceps that were driven by a constant pneumatic pressure, as described previously (Magill et al. 2006). However, we did not analyze neuronal activity recorded concurrently with these sensory stimuli. Because the analyzed activity was recorded at least several minutes after the cessation of the brief pinch, it was also considered as spontaneous. The animals did not exhibit either a marked change in the electrocardiogram or respiration rate, and did not exhibit a hindpaw withdrawal reflex, in response to the pinch. Moreover, withdrawal reflexes were not present during episodes of spontaneous and/or prolonged cortical activation, thus indicating anesthesia was adequate throughout the recordings.

Juxtacellular Labeling of Single Neurons

To identify the somatodendritic architecture and locations of some of the recorded thalamic units, single neurons were selectively labeled with Neurobiotin by the juxtacellular method (Pinault 1996; Magill et al. 2000). Briefly, the electrode was advanced slowly toward the neuron while a microiontophoretic current was applied (1–10 nA positive current; 200 ms duration; 50% duty cycle). The optimal position of the electrode for cell labeling was identified when the firing pattern of the neuron was robustly modulated by the current injection. Neuronal firing was modulated by the microiontophoretic current for 2–30 min to obtain reliable labeling. This single-unit entrainment resulted in just one neuron being labeled with Neurobiotin. The Neurobiotin was then left to transport along neuronal processes for up to 8 h. After the recording and labeling sessions, the animals were given a lethal dose of ketamine (150 mg/kg) and perfused transcardially with 100 mL of 0.05 M phosphate-buffered saline (PBS), pH 7.4, followed by 300 mL of 0.1% w/v glutaraldehyde and 4% w/v paraformaldehyde in 0.1 M phosphate buffer (PB), pH 7.4 and then by 200 mL of 4% w/v paraformaldehyde in PB. Brains were then left in the latter fixative solution at 4 °C until sectioning 24–72 h later. Sixty-four of the thalamic neurons detailed herein were juxtacellularly labeled. These Neurobiotin-labeled neurons were designated "identified" and precisely localized to different input zones of the motor thalamus (see below). The remaining (unlabeled) thalamic neurons ($n = 85$) were also included because, using stereotaxy and readouts from the stepper motor, we could accurately extrapolate their locations from those of identified neurons (recorded with the same glass electrodes in the same animals). Henceforth, we designate these unlabeled neurons as "extrapolated."

Histology, Immunofluorescence, and Microscopy

The fixed brains were cut into 50-μm thick sections in the parasagittal plane on a vibrating microtome (VT1000S; Leica Microsystems). All the following incubations were performed at room temperature. To visualize the Neurobiotin-filled neurons, free-floating sections were washed in PBS and incubated overnight in Cy3-conjugated streptavidin (1:1000; PA43001, GE Healthcare) in "Triton-PBS" (PBS containing 0.3% v/v Triton X-100 [Sigma]). After washing, the sections were mounted on glass slides, coverslipped, and examined with an epifluorescence microscope (AxioPhot, Zeiss) to identify Neurobiotin-filled neurons. To delineate thalamic nuclei and map the location of each identified neuron (Fig. 1), we subsequently incubated sections containing the fluorescently labeled somata overnight with a primary antibody mixture of rabbit anti-vesicular glutamate transporter 2 (VGluT2; 0.4 μg/mL of affinity-purified IgG; Hioki et al. 2003; a gift from Prof. Takeshi Kaneko, Kyoto University) and mouse anti-glutamic acid decarboxylase of 67 kDa (GAD67; 2 μg/mL; MAB5406, Millipore) in Triton-PBS containing 1% v/v donkey serum (Jackson Immunoresearch; all the following antibody incubations were carried out

with the same buffer). After washing with PBS, the sections were incubated for 2–4 h with a mixture of fluorophore-conjugated secondary antibodies (all raised in donkey): Anti-rabbit IgG (DyLight 649, 1:200; Jackson Immunoresearch) and anti-mouse IgG (Alexa Fluor 488, 1:200; Life Technologies). When necessary, the adjacent sections were incubated with NeuroTrace 500/525 (1:150; N-21480; Life Technologies), a green fluorescent Nissl stain, in Triton-PBS for 30 min to visualize cytoarchitecture. After washing, the fluorescently labeled sections were mounted on glass slides, coverslipped, and examined with a laser-scanning confocal microscope (LSM710, Zeiss). To precisely localize the recorded neurons to distinct thalamic nuclei, fluorescent images of the thalamus around the Neurobiotin-filled neurons were taken at a low magnification with a ×5 objective lens (EC Plan-Neofluar, numerical aperture 0.16; Zeiss), a pinhole thoroughly opened (i.e. in "non-confocal" mode), and a zoom factor of 0.6. Appropriate sets of laser beams and emission windows were used for Alexa Fluor 488 (excitation 488 nm, emission 492–544 nm), Cy3 (excitation 543 nm, emission 552–639 nm), and DyLight 649 (excitation 633 nm, emission 639–757 nm). Images of each of the channels were taken sequentially and separately to negate possible "bleed through" of signal across channels. Images were combined into montages (Fig. 1) and, when necessary, images from the adjacent sections were overlaid and aligned in Illustrator software (Adobe CS3, Adobe Systems). The 2 input zones of the motor thalamus were delineated on the basis of their distinctive distributions of VGluT2 and GAD67 immunoreactivities (see below and Kuramoto et al. 2009, 2011). Only identified neurons located >50 μm away from the borders of BZ or CZ were analyzed. Extrapolated neurons had to be located >100 μm away from these borders to be included in the analyses. The dendrites of neurons in the rat motor thalamus only rarely radiate >200 μm from the parent somata (Kuramoto et al. 2009). Thus, most of the proximal dendrites of our neurons were likely to be confined to just one zone.

For qualitative comparison of the distributions of different axon terminal markers in the motor thalamus (Supplementary Fig. 1), parasagittal tissue sections from an adult rat (370 g; not used for electrophysiology) were prepared as described above and adjacent sections were immunofluorescently labeled according to 1 of 2 protocols (A or B). Thus, the sections were incubated overnight with a mixture of either: (A) Mouse anti-GAD67 (2.0 μg/mL), guinea pig anti-vesicular glutamate transporter 1 (VGluT1; 1.0 μg/mL; Fujiyama et al. 2001; a gift from Prof. Takeshi Kaneko, Kyoto University), and rabbit anti-VGluT2 (1.0 μg/mL) or (B) rabbit anti-vesicular acetylcholine transporter (VAChT; 1:10 000; V-5387, Sigma) and guinea pig anti-parvalbumin (PV; 1:1000; 195004, Synaptic Systems). After washing, the sections were further incubated overnight with a mixture of fluorophore-conjugated secondary antibodies (raised in donkey): either (A) anti-mouse IgG (Alexa Fluor 488, 1:200), anti-guinea pig IgG (Cy3, 1:200; Jackson Immunoresearch), and anti-rabbit IgG (DyLight 649, 1:200) or (B) anti-rabbit IgG (Cy3, 1:500; Jackson Immunoresearch) and anti-guinea pig IgG (DyLight 649, 1:200; Jackson Immunoresearch). After washing, the sections that had been processed using the protocol B were incubated with the fluorescent Nissl stain as detailed above. For anatomical mapping of the locations of all recorded cells throughout the motor thalamus (Fig. 2 and Supplementary Fig. 2), parasagittal sections from another rat (330 g) were prepared, and one in every 2 sections through the thalamus were processed for triple fluorescence labeling. Sections were first incubated with a mixture of rabbit anti-VGluT2 (0.4 μg/mL) and mouse anti-GAD67 (2 μg/mL) antibodies. After washing, the sections were incubated overnight with a mixture of fluorophore-conjugated secondary antibodies (raised in donkey): Anti-rabbit IgG (DyLight 649, 1:200) and anti-mouse IgG (Cy3, 1:200). Finally, the sections were incubated with the green fluorescent Nissl stain as detailed above.

After montage images of the thalamus were created as above, the cytoarchitecture of thalamic nuclei (Paxinos and Watson 2007) was compared with the distributions of VGluT2, GAD67, and other immunoreactivities on the same sections (Fig. 1 and Supplementary Figs 1 and 2). Confocal images at a high magnification were taken with a ×100 oil-immersion objective lens (alpha Plan-Apochromat DIC M27, numerical aperture 1.46; Zeiss), a pinhole of 1.0 Airy unit, and a zoom factor of 3. The excitation laser beams and emission filters used were the same as those detailed above (for the Nissl stain we used the same settings as those for visualizing Alexa Fluor 488).

Nomenclature of Motor Thalamic Nuclei and Delineation of Input Zones

In rat motor thalamus, distinguishing the border between VA and VL on the basis of cytoarchitecture (i.e. labeling of Nissl substance) is difficult (Fig. 1*A*). As such, they have often been treated as a single nuclear mass called the "VA–VL complex" or "VAL" (Fig. 1*A*; Groenewegen and Witter 2004; Jones 2007; Paxinos and Watson 2007). Defining the border between VA–VL and VM is similarly difficult using labeling for Nissl substance and cytoarchitectonic criteria, at least in the parasagittal plane (Fig. 1*A*). As previously reported (Kuramoto et al. 2009, 2011), VM and the rostroventral portion of the VA–VL complex, but not the caudodorsal portion of the VA–VL complex, contained numerous, densely packed GAD67-immunoreactive (GAD67+) axon terminal-like puncta, which were often relatively large (2–4 μm in the longest axis; Fig. 1*B*). In contrast, the caudodorsal portion of the VA–VL complex, but not VM or the rostroventral portion of VA–VL, contained numerous VGluT2 + axon terminal-like puncta, many of which were very large (>5 μm; Fig. 1*C*). These distinctly distributed groups of "large" GAD67 + axon terminals and "giant" VGluT2 + axon terminals originate from GABAergic basal ganglia output nuclei and glutamatergic cerebellar nuclei, respectively (Kuramoto et al. 2011). Thus, while complementary patterns of GAD67 and VGluT2 immunoreactivities do not respect traditional cytoarchitectonic boundaries, they do parcellate the motor thalamus into a BZ and a CZ (compare solid and dashed lines in Fig. 1*A*–*C*). For simplicity, we hereafter refer to the rostroventral portion of the VA–VL complex (demarcated by dense GAD67 immunoreactivity) and caudodorsal portion of the VA–VL complex (demarcated by dense VGluT2 immunoreactivity) as VA and VL, respectively. Accordingly, BZ is composed of VA and VM, whereas CZ corresponds to VL (Fig. 1*B*,*C*).

Electrophysiological Data Analysis

All biopotentials were digitized on-line using a Power1401 Analog-Digital converter (Cambridge Electronic Design) and PC running Spike2 acquisition and analysis software (version 7; Cambridge Electronic Design). Unit activity and the ECoG were sampled at 17.9 kHz. Data from the recording session were visually inspected and epochs of robust cortical SWA or cortical activation were selected according to the previously described characteristics of these brain states (Magill et al. 2001, 2006). Power spectra of ECoGs were calculated with frequency resolutions of 0.25 and 2.0 Hz for SWA and cortical activation, respectively, using the MATLAB (MathWorks) toolbox Neurospec 2.0 (http://www.neurospec.org). A 100 s portion of the spike train recorded during each defined brain state was isolated and used for statistical analyses. Putative single-unit activity was isolated with standard "spike sorting" procedures (Mallet et al. 2008), including template matching, principal component analysis, and supervised clustering (Spike2). Isolation of a single unit was verified by the presence of a distinct refractory period in the interspike interval (ISI) histogram. Only neurons in which <1% of all ISIs were <2 ms were analyzed in this study. For further analysis, single-unit activity was converted so that each spike was represented by a single digital event (Spike2). The mean firing rate (spikes/s) was calculated from the total number of spikes per 100 s data epoch. The coefficient of variation of the ISIs, a value used widely as an indicator of regularity in point processes (Johnson 1996), was also calculated.

Detection of Low-Threshold Ca^{2+} Spike Bursts

Low-threshold Ca^{2+} spike (LTS) bursts are discharged by thalamic projection neurons of various species during anesthesia, natural sleep, and quiet wakefulness (Fanselow et al. 2001; Swadlow and Gusev 2001; Ramcharan et al. 2005; Llinás and Steriade 2006). Previous quantitative analyses have shown that LTS bursts are preceded by a silent period (50–100 ms; Lu et al. 1992). LTS bursts were classified as such using custom Spike2 scripts, according to previously defined

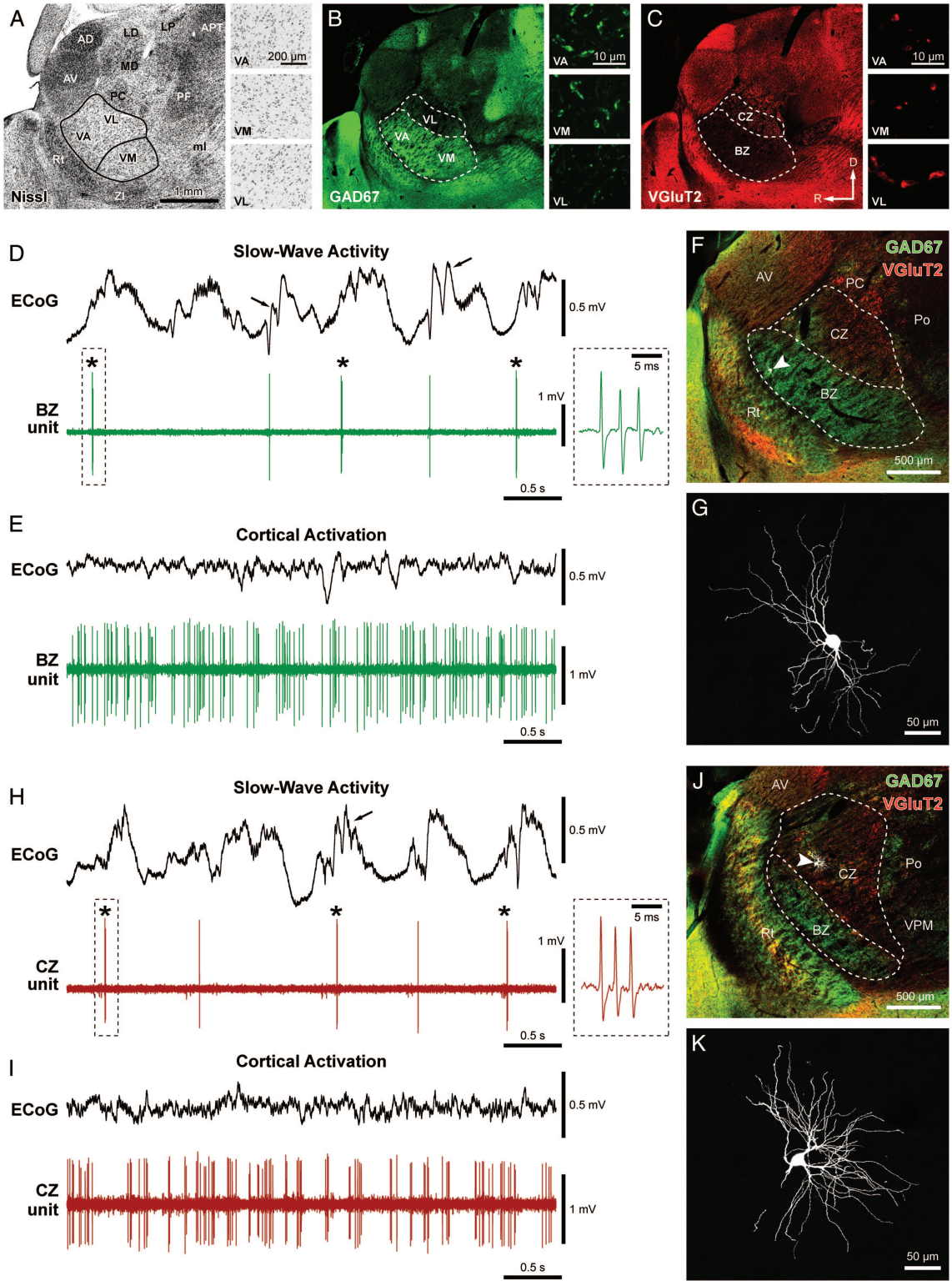

Figure 1. Typical spike firing patterns and somatodendritic structure of identified neurons in the BZ and CZ of the motor thalamus. (*A–C*) Matched fluorescence images of Nissl labeling (*A*; inverted tone) and immunoreactivities for GAD67 (*B*) and VGluT2 (*C*) at the level of motor thalamus (VA, VM, and VL nuclei) in parasagittal view. "Standard" cytoarchitectonic borders of VM and the VA–VL complex (black lines in *A*) were extrapolated from an atlas (Paxinos and Watson 2007; ~1.5 mm lateral from Bregma). These nuclei have similar cytoarchitecture (insets in *A*). GAD67 and VGluT2 immunoreactivities (in a section immediately adjacent to that in *A*) do not respect these cytoarchitectonic boundaries but do show complementary patterns in the motor thalamus; GAD67 is more intense ventrally (*B*), whereas VGluT2 is more evident dorsally (*C*). (*B* and *C* insets) High-magnification confocal images of immunoreactivity in VA, VM, and VL. Note: GAD67-immunoreactive punctate profiles are larger and denser in VA and VM compared with VL (*B*), whereas VGluT2-immunoreactive puncta are much larger and denser in VL compared with VA and VM (*C*). Thus, a BZ, corresponding to VA and VM nuclei, is delineated by GAD67 immunoreactivity, whereas a CZ, corresponding to VL, is delineated by VGluT2 immunoreactivity. BZ and CZ borders are indicated with dashed lines in *B* and *C*. (*D* and *E*) Spontaneous activity of a thalamic unit recorded in the BZ during SWA (*D*) and cortical activation (*E*), as defined by simultaneous ECoG recordings. Spindle oscillations (7–12 Hz; arrows) were often superimposed on cortical slow (~1 Hz) oscillations (*D*). During SWA, LTS bursts (indicated with asterisks) were fired on most cycles of the slow

criteria for identifying the LTS bursts in extracellular unit recordings (Lacey et al. 2007): 1) At least 2 action potentials with an ISI of ≤5 ms but with a preceding silent period of >100 ms (Lu et al. 1992) and 2) a maximum ISI of 10 ms was used to define the end of a LTS burst (Fanselow et al. 2001).

Phase Analysis with the Hilbert Transform

To investigate how the activity of individual thalamic neurons varied in time with respect to ongoing cortical network activity during SWA, we analyzed the instantaneous phase relationships between thalamic spike times and cortical oscillations in specific frequency bands. Signal conditioning and analyses were performed using MATLAB. ECoG signals containing 100 s of robust SWA were first filtered at either slow oscillation (0.4–1.6 Hz) or spindle oscillation (7–12 Hz) frequencies using a neutral-phase bandpass filter (Butterworth filter, 3 poles). These frequency ranges were chosen according to previous studies utilizing this animal model (Magill et al. 2004; Mallet et al. 2008). Subsequently, the instantaneous phase and power of the ECoG were calculated from the analytic signal obtained via the Hilbert transform (Lachaux et al. 1999; Le Van Quyen et al. 2001). In this formalism, peaks in the ECoG oscillations correspond to a phase of 0° and troughs to a phase of 180°. Linear phase histograms, circular phase plots, and circular statistical measures were calculated using the instantaneous phase values for each spike, only the first spike in each LTS burst, or all spikes outside of LTS bursts (non-LTS spikes), depending on the frequency band being analyzed. For phase analysis in the spindle-frequency range, a spike phase value was only included when the spike occurred during a period that exceeded a threshold of ≥0.5 standard deviation of the mean instantaneous power at 7–12 Hz, a criterion that appeared to best capture the periods of increased spindle oscillation. Descriptive and inferential circular statistics were then calculated using the CircStat toolbox (Berens 2009) for MATLAB and Oriana software (Kovach Computing Services). For the calculation of vector lengths and statistical comparisons, we included only those neurons that fired ≥40 spikes (or LTS bursts) during the entire recording (for analysis of slow oscillations) or during "suprathreshold periods" (for spindle oscillations). These neurons were then tested for significantly phase-locked firing (defined as having $P < 0.05$ in Rayleigh's Uniformity Test). The null hypothesis for Rayleigh's test was that the spike data were distributed in a uniform manner. We and others have previously remarked that the non-sinusoidal nature of some field potential oscillations, such as the cortical slow oscillation, can confound standard circular statistics, particularly Rayleigh's test (Siapas et al. 2005; Mallet et al. 2008; Sharott et al. 2012). Thus, for the analysis of thalamic neuron firing relationships with cortical slow oscillations, Rayleigh's tests were only carried out after any phase non-uniformities of the slow oscillations were corrected with the empirical cumulative distribution function (Siapas et al. 2005). For each of the neurons that were significantly phase-locked, the mean phase angle was calculated. Differences in the mean phase angles of groups of neurons were tested by the Watson–Williams F-test ($P < 0.05$ for significance). Differences in overall phase distributions were tested by the Mardia-Watson-Wheeler test ($P < 0.05$ for significance). The mean resultant vector length (referred to hereafter as simply "vector length") of the phase distribution, bound between zero and one (the closer to one, the more concentrated the angles), was used to quantify the level of phase-locking around the mean angle, and differences between the vector lengths of 2 groups were tested by the Mann–Whitney U-test. Where data are displayed in circular plots (Figs 5 and 6) lines radiating from the center are the vectors of the preferred phases of firing (with the center and perimeter of the circle representing vector lengths of 0 and 1, respectively). The small open circles on the perimeter represent the phase values of LTS burst onsets (Fig. 5*H*) or the preferred phases of each neuron otherwise.

Non-circular Statistical Tests

The Shapiro-Wilk test was used to judge whether noncircular data sets were normally distributed ($P \leq 0.05$ to reject for parametric tests). Because some data sets were not normally distributed, we employed nonparametric statistical testing throughout (SigmaPlot 12; Systat Software). The Mann–Whitney U-test was thus used for the comparisons of unpaired data. The minimum significance level for statistical tests was taken to be $P < 0.05$. More conservative significance levels are as stated in the text. Data are expressed as mean ± standard error of the mean (SEM) in the text unless stated otherwise.

Results

Delineation of Constituent Nuclei of the Rat Motor Thalamus, and Functional Parcellation into BZ and CZ

In this study, we endeavored to advance understanding of motor thalamocortical operations by accounting for the activities of individual (identified) neurons in distinct areas of motor thalamus that are structurally and functionally defined according to discrete inputs. To this end, and following Kuramoto et al. (2009, 2011), we used markers of specific groups of GABAergic axon terminals or glutamatergic axon terminals (i.e. GAD67 and VGluT2, respectively) to define the boundaries of VA, VL, and VM, as well as to parcellate the motor thalamus into the BZ and the CZ (Fig. 1*A*–*C*). Here, we define the BZ to be composed of VA and VM, whereas the CZ corresponds to VL (Fig. 1*B*,*C*; see Materials and Methods). Our simplifying nomenclature, which is based on subcortical afferents, is conceptually in line with that previously proposed for monkey motor thalamus (Ilinsky and Kultas-Ilinsky 1987, 2002) and human motor thalamus (Kultas-Ilinsky et al. 2011).

Immunoreactivities for GAD67 and VGluT2 delineate the BZ and CZ. For comparison, we also tested whether markers for other major inputs to the motor thalamus could be similarly useful for functional parcellation (Supplementary Fig. 1). We first assessed immunoreactivities for VGluT1 and VAChT, markers of the axon terminals of glutamatergic cortical neurons, and cholinergic neurons, respectively. VGluT1+ puncta are typically small (<1 μm), abundant, and homogeneously distributed across VA, VL, and VM (Supplementary Fig. 1*D* and see Kuramoto et al. 2011). Punctate VAChT immunoreactivity was very sparsely and uniformly distributed in the motor thalamus (Supplementary Fig. 1*E*). We also found that immunoreactivity for parvalbumin in neuropil, a good indicator of inputs from GABAergic thalamic reticular nucleus

oscillation. Such bursts were characterized by up to 6 spikes fired in rapid succession (instantaneous intraburst rate >150 spikes/s), with a progressive increase in ISIs and attenuation of spike amplitude during the burst (typical burst is highlighted by the dashed box and also shown at higher temporal resolution in the inset). (*F*) After recording, the neuron was juxtacellularly filled with Neurobiotin, fluorescently labeled and identified (white, arrowhead), and then localized to BZ, demarcated by intense GAD67 immunoreactivity (green) and sparse VGluT2 immunoreactivity (red) in the parasagittal section (lateral ~1.8 mm). (*G*) Magnified view of the same identified neuron, which had "bushy" dendrites typical of thalamic projection neurons. (*H* and *I*) Spontaneous activity of a thalamic unit recorded in the CZ of another rat during SWA (*H*) and cortical activation (*I*). (*J*) The same neuron was juxtacellularly labeled and identified (white, arrowhead) and then localized to CZ, delineated by sparse GAD67 (green) and moderate VGluT2 (red) immunoreactivities in the parasagittal section (lateral ~2.1 mm). (*K*) Magnified view of the same neuron. AD, anterodorsal nucleus; APT, anterior pretectal nucleus; AV, anteroventral nucleus; LD, laterodorsal nucleus; LP, lateroposterior nucleus; MD, mediodorsal nucleus; ml, medial lemniscus; PC, paracentral nucleus; PF, parafascicular nucleus; Po, posterior nuclear complex; Rt, thalamic reticular nucleus; VA, ventral anterior nucleus; VL, ventral lateral nucleus; VM, ventral medial nucleus; VPM, ventral posteromedial nucleus; ZI, zona incerta. R, rostral; D, dorsal. Scale bar in *A* also applies to low-magnification images in *B* and *C*. The 3 insets in each panel (*A*, *B*, or *C*) share the same scale.

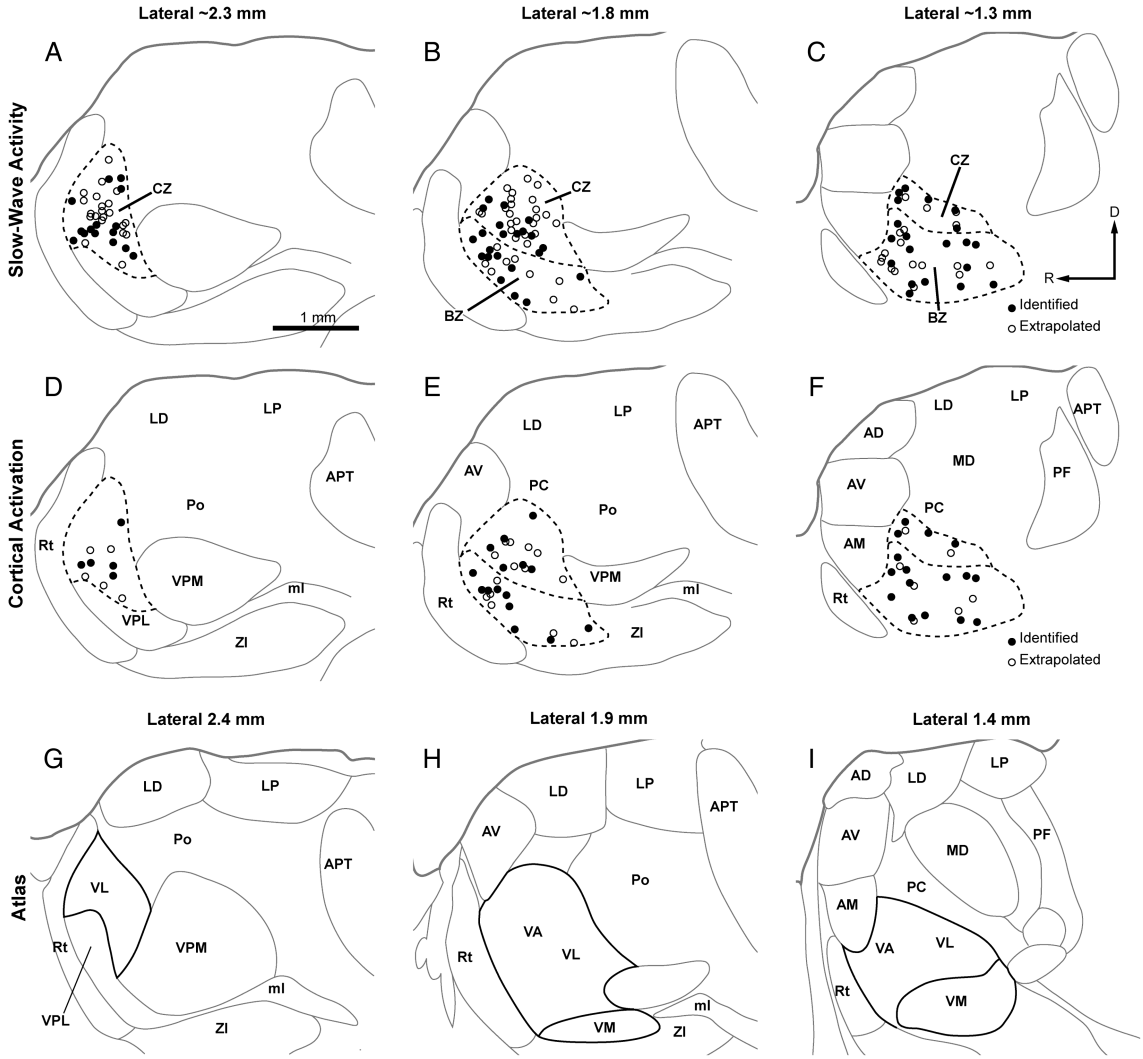

Figure 2. Localization of all recorded thalamic neurons to BZ and CZ. (*A–F*) Parasagittal views of the locations of identified and extrapolated neurons recorded during either SWA (*A–C*) or cortical activation (*D–F*), as plotted at 3 different mediolateral planes; ~2.3 mm (*A* and *D*), ~1.8 mm (*B* and *E*), and ~1.3 mm (*C* and *F*) lateral to Bregma. Borders between nuclei in *A–F* were omitted when they could not be unambiguously delineated with labeling for Nissl substance, GAD67, or VGluT2. (*G–I*) Delineation of thalamic nuclei according to the closest 3 parasagittal planes available (lateral from Bregma: 2.4, 1.9, and 1.4 mm) in a widely used rat brain atlas (Paxinos and Watson 2007). Note that the boundaries of the BZ and CZ, (dashed lines) do not match nuclear borders delineated in the atlas on cytoarchitectonic grounds (solid black lines). AM, anteromedial nucleus; VPL, ventral posterolateral nucleus; abbreviations for other thalamic nuclei are defined in Figure 1. R, rostral; D, dorsal. Scale bar in *A* also applies to all other panels.

(Rt) neurons (Arai et al. 1994), was densely and homogeneously distributed across the 2 input zones (Supplementary Fig. 1*F*). These qualitative observations together suggest that, unlike in the case of afferents from basal ganglia and cerebellar nuclei, glutamatergic cortical inputs, cholinergic inputs (likely from the brainstem), and presumed GABAergic inputs from Rt are similarly distributed across the motor thalamus and thus, do not readily parcellate it into distinct input zones.

Cortical Activity

We recorded and labeled individual thalamic neurons located in BZ and CZ, parcellated on the basis of complementary GAD67 and VGluT2 immunoreactivities, with a view to characterizing the similarities and differences in their spontaneous activities. In doing so, we paid particular attention to distinct brain states and the cortical network oscillations that define them. Thalamic projection neurons can operate in 2 functionally distinct firing modes, "tonic" or "bursting," according to brain state and the requirements of ongoing information processing (Sherman 2001a; Llinás and Steriade 2006). It was thus imperative to record the ipsilateral ECoG simultaneously with the activity of individual motor thalamic neurons in order to provide context, that is, to analyze thalamic activity according to ongoing brain state. We focused our analyses on thalamic unit activity recorded during 2 well-defined brain states, SWA (Fig. 1*D*,*H*) and "cortical activation" (Fig. 1*E*,*I*), evident in urethane-anesthetized rats (see Materials and Methods).

Spontaneous Activities of Identified Motor Thalamic Neurons

We recorded a total of 149 single units in the motor thalamus, 64 of which were unequivocally identified, that is, after electrophysiological characterization, they were juxtacellularly labeled with Neurobiotin, and their somata were precisely localized to BZ or CZ according to GAD67 and VGluT2

Table 1
Number of neurons analyzed in the rat motor thalamus in each brain state

Zone	Nucleus	Slow-Wave Activity		Cortical Activation	
		Identified	Extrapolated	Identified	Extrapolated
BZ	VA and VM	25	23	21	11
	VA[a]	12	13	10	6
	VM[a]	7	6	6	4
CZ	VL	32	48	15	15

[a]For a comparative analysis between VA and VM neurons (Fig. 7), we divided the BZ according to a "virtual border". Neurons within 200 μm of this virtual border were excluded from the comparative analysis of VA and VM, but included in analyses of the BZ as a whole. See main text for details and definition of abbreviations.

immunoreactivities (Figs 1 and 2; Table 1). During periods of robust SWA in ipsilateral frontal cortex, the activity of identified BZ neurons was typified by a relatively low mean firing rate (<4 spikes/s) and a propensity to fire discrete bursts of spikes (Fig. 1*D*). These bursts were exemplified by 2–6 spikes fired in rapid succession (instantaneous intraburst rates of >150 spike/s), with a progressive decrease in spike amplitude (Fig. 1*D*, inset). Many of these bursts satisfied the criteria for stereotypical low-threshold Ca^{2+} spike (LTS) bursts (see Materials and Methods). Moreover, spikes were often fired in time with cortical slow (~1 Hz) oscillations and related spindle (7–12 Hz) activities (Fig. 1*D*). In contrast, during cortical activation, the activity of identified BZ neurons was typified by relatively high mean firing rates (>10 spikes/s) and a "tonic" irregular firing pattern (Fig. 1*E*). The spikes that were fired tonically at high rates during activation were often of smaller amplitudes than the spikes fired by the same neurons during SWA (Fig. 1*D*,*E*). Importantly, the activity of identified neurons of CZ was qualitatively similar to that of neurons of BZ, irrespective of brain state (Fig. 1*H*,*I*). In line with their similar activities, Neurobiotin-labeled neurons in both zones (Fig. 1*F*,*J*) had the "bushy" or "tufted" dendrites (Fig. 1*G*,*K*) that are typical of projection neurons in the mammalian motor thalamus (Yamamoto et al. 1984; Kuramoto et al. 2009; Tlamsa and Brumberg 2010).

Firing Rates and Propensity to Fire LTS Bursts are Similar for Neurons in the BZ and CZ

We next quantitatively compared the basic firing properties of all neurons recorded in BZ and CZ. For the following analyses, we pooled together all identified and "extrapolated" neurons, that is, the unlabeled neurons whose locations could be accurately extrapolated from those of identified neurons (see Materials and Methods; Table 1), because their respective activities were indistinguishable (data not shown). Anatomical mapping showed that the full mediolateral extent of the 2 zones could be unambiguously defined with GAD67 and VGluT2 immunoreactivities (Supplementary Fig. 2) and, importantly, that we sampled neurons located throughout both zones (Fig. 2*A*–*F*). The same anatomical analyses also served to reinforce the idea that GAD67 and VGluT2 immunoreactivities, and thus the boundaries of the 2 distinct input zones, do not conform to standard cytoarchitectonic boundaries (Fig. 2 and Supplementary Fig. 2).

Despite the contrasting excitatory and inhibitory inputs of the 2 zones, the mean firing rates of BZ and CZ neurons were similar when compared during either SWA or cortical

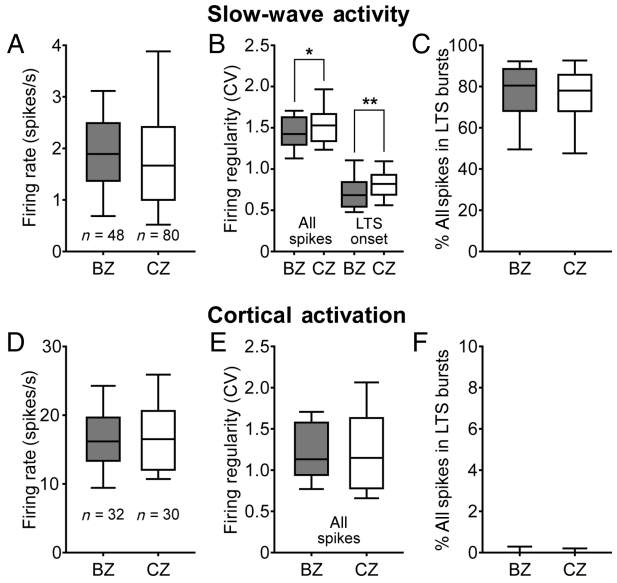

Figure 3. Quantitative comparisons of firing rates and patterns of thalamic neurons in BZ and CZ according to brain state. Mean firing rates (*A* and *D*), firing regularities, as measured by the coefficients of variation (CV) of ISIs (*B* and *E*), and mean percentage of all spikes occurring in LTS bursts (*C* and *F*) for all neurons recorded in the BZ and in the CZ. (*A*–*C*) Thalamic activity parameters during SWA. Firing regularity during SWA was separately defined for all spikes and for the onset times of LTS bursts (*B*). (*D*–*F*) Activity parameters during cortical activation. Although the firing rates and patterns of motor thalamic neurons were highly brain state dependent, BZ and CZ neurons did not differ in their mean firing rates or propensity to fire LTS bursts. Note that LTS bursts were rare during cortical activation. Box plots in this and subsequent figures denote the 10th and 90th percentiles (whiskers), interquartile range, and medians. *n*, the number of recorded neurons. $*P = 0.049$; $**P = 0.005$ (both Mann–Whitney *U*-tests).

activation (Fig. 3*A*,*D*). Although there was a small, barely significant difference in the regularities of all spikes fired by BZ and CZ neurons during SWA (Fig. 3*B*), firing regularities were similar during cortical activation (Fig. 3*E*). We next analyzed the occurrence of the distinctive LTS bursts of neurons in both input zones. During SWA, all motor thalamic neurons fired numerous LTS bursts ~75% of all spikes fired by BZ and CZ neurons during SWA occurred within LTS bursts. The onset times of the LTS bursts of BZ neurons were slightly more regular than those of CZ neurons (Fig. 3*B*), but there was no difference in the propensity to fire LTS bursts across the zones (Fig. 3*C*).

The activities of neurons in the both zones showed clear brain state dependency, shifting from sparse burst firing to tonic irregular spiking upon transition from SWA to cortical activation. The mean firing rates of both BZ and CZ neurons were markedly higher during cortical activation than during SWA (Fig. 3*A*,*D*; both $P < 0.001$, Mann–Whitney *U*-tests). Firing regularities of all spikes also increased during cortical activation (Fig. 3*B*,*E*; both $P < 0.01$, Mann–Whitney *U*-tests), likely reflecting a significant decrease in LTS bursting by both groups of neurons (Fig. 3*C*,*F*; both $P < 0.001$, Mann–Whitney *U*-tests). Indeed, during activated brain states, the proportions of all spikes included in LTS bursts were very low, though not zero, for neurons in both zones (Fig. 3*F*). These data show that motor thalamic neurons in both zones tend to fire in bursting and tonic modes during SWA and cortical activation, respectively, as perhaps could be predicted (Llinás and Steriade 2006).

In summary, the contrasting GABAergic and glutamatergic afferents of BZ and CZ were not reflected by differences in the firing rates or propensity to fire LTS bursts of the neurons therein, irrespective of brain state.

Dynamics of the LTS Bursts of Thalamic Neurons in the BZ and CZ are Different

Although the propensity for neurons in the 2 input zones to fire LTS bursts is similar, this does not rule out the possibility that the structure of the LTS bursts is different. Thus, we next examined the fine dynamics of the LTS bursts (Fig. 4). The mean ISI of the LTS bursts of BZ neurons was significantly longer than that of CZ neurons (Fig. 4*A*; also see insets in Fig. 1*D*,*H*). The mean duration of the LTS bursts of BZ neurons was also significantly longer than that of CZ neurons (Fig. 4*B*). This different duration may be best accounted for by the longer mean ISIs of bursts fired by BZ neurons because, on average, the number of spikes per LTS burst were similar for the neurons of each zone (Fig. 4*C*). Despite the similarity in the average number of spikes per burst, there were differences in the proportions of LTS bursts containing different numbers of spikes; CZ neurons tended to fire LTS bursts of 2 spikes more often than BZ neurons, whereas BZ neurons fired LTS bursts of 3 spikes more commonly than CZ neurons (Fig. 4*D*). The LTS bursts fired by a variety of thalamic projection neurons are often associated with a progressive increase in ISIs (as the burst evolves), and the duration of the first ISI in a given burst is predictive of the total number of action potentials to be subsequently fired (Domich et al. 1986; Jeanmonod et al. 1996; Lacey et al. 2007; Slézia et al. 2011). Our analyses showed that ISIs increased during the LTS bursts fired by thalamic neurons of both zones (Fig. 4*E*, *F*). Moreover, the first ISI in a burst was predictive of the total number of spikes within a burst; the relationship between the 2 parameters was well fit by a single exponential decay curve for each group of neurons (Fig. 4*G*). Moreover, the data from BZ and CZ neurons were clearly and significantly separated from each other (Fig. 4*G*; 2-way analysis of variance on ranks followed by post hoc Tukey tests: $P < 0.001$ between BZ and CZ neurons for LTS bursts of 2–5 spikes, and $P = 0.052$ for LTS bursts of 6 spikes). Finally, the normalized ISI histograms for all spikes in all LTS bursts of BZ and CZ neurons showed partially overlapping, unimodal distributions with distinct peaks at ~3.4 and ~2.4 ms, respectively (Fig. 4*H*).

Together, these data show that while thalamic neurons in the 2 input zones share some features of LTS bursting, they differ in fine dynamics such that each group favors bursts with different spike counts and, most strikingly, BZ neurons fire slower LTS bursts than CZ neurons.

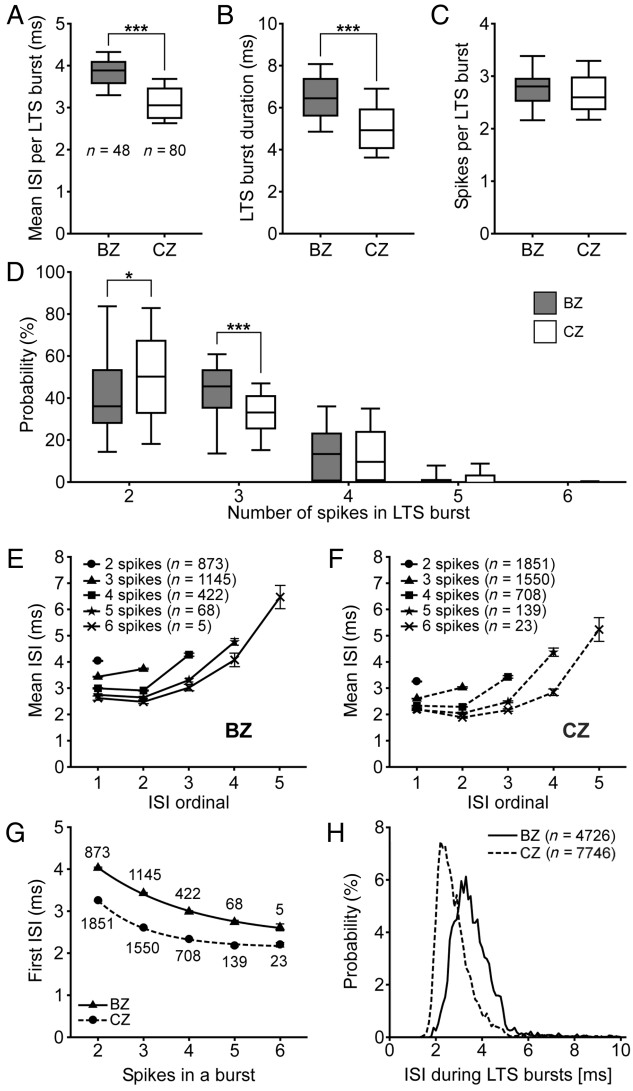

Figure 4. Neurons in BZ and CZ have different LTS bursts. (*A–C*) Mean ISI per burst (*A*), mean burst duration (*B*), and mean number of spikes per LTS burst (*C*). Note that neurons in the BZ fire slower and longer LTS bursts than those in the CZ. *n*, the number of neurons analyzed. (*D*) CZ neurons tended to fire LTS bursts of 2 spikes more often than BZ neurons, whereas BZ neurons fired LTS bursts of 3 spikes more commonly than CZ neurons. (*E* and *F*) Plots of ISIs as a function of the number of spikes in the LTS burst. *n*, the number of bursts analyzed. Note the progressive increases in ISI durations as the bursts evolve. (*G*) For both groups of neurons, the duration of the first ISI in a given burst was highly predictive of the total number of spikes to be subsequently fired ($R^2 > 0.99$ for both exponential decay curves). (*H*) Normalized ISI histograms (0.1 ms bins) for all spikes in all LTS bursts. Note the 2 unimodal distributions for BZ and CZ neurons only partially overlap and have distinct peak values. *n*, the number of ISIs analyzed. Data in *E–G* are mean ± SEM. $^*P < 0.05$; $^{***}P < 0.001$ (Mann–Whitney *U*-tests).

Distinct Temporal Coupling of Neuronal Activity in the BZ and CZ with Cortical Slow Oscillations

Neurons in functionally related nuclei of the rat somatosensory thalamus are better distinguished by the temporal coupling of their activity to cortical rhythms than by their spontaneous firing rates (Slézia et al. 2011). Thus, while the firing rates of BZ and CZ neurons were similar, nucleus-specific differences in other facets of temporal activity could still arise. During SWA, the single spikes and LTS bursts of motor thalamic neurons were often fired in time with cortical slow oscillations and spindle oscillations (Fig. 1*D*,*H*). We tested whether the contrasting inputs of the 2 thalamic zones are reflected by differences in the temporal coupling of the constituent neuronal activity to these cortical oscillations. We first quantified the strength and distribution of phase-locked thalamic firing in relation to cortical slow oscillations in the frontal ECoG (Fig. 5). The power of the frontal ECoGs recorded with BZ or CZ neurons was similar (Fig. 5*A*), and plots of the relative power in the spike trains of BZ neurons and CZ neurons exhibited similar peaks in power in the 0.4–1.6 Hz band (Fig. 5*B*). Accordingly, the spike discharges

of BZ and CZ neurons were both significantly coherent with the cortical slow oscillations (Fig. 5*C*). However, the coherence between BZ neurons and cortex was approximately twice that between CZ neurons and cortex (Fig. 5*C*; $P < 0.001$, Mann–Whitney *U*-test), thus providing a first indication that the activity of neurons in BZ is more tightly coupled to cortical slow oscillations.

To further examine the temporal relationship between activity in the motor thalamus and the cortex, we analyzed the instantaneous phase of thalamic neuron spiking with respect to ECoGs. When the entire spike train of each neuron was analyzed, both BZ and CZ neurons ($n = 48$ and 80, respectively) preferentially fired at the ascending phase of cortical slow oscillations (Fig. 5*D*), that is, at around the phase that cortical neurons transition from silence to coordinated firing (Sakata and Harris 2009; Chauvette et al. 2010). The peak of activity of BZ neurons was larger and narrower in the histogram, again indicating tighter phase-locking as a population (Fig. 5*D*). We further investigated this possibility using circular statistical analyses. To qualify for these analyses, a neuron had to fire ≥40 spikes during the 100 s recording, a first sampling criterion that helped to ensure accurate determination of circular means and the significance of any phase-locked firing. The spikes of nearly all the qualifying neurons were significantly locked to the slow oscillations (BZ, 48 of 48 qualifying neurons; CZ, 76 of 77 qualifying neurons; $P < 0.05$, Rayleigh's Uniformity Tests). Circular plots of the preferred phases of these individual phase-locked neurons also demonstrated their strong tendency to fire at the ascending phase of the slow oscillations (Fig. 5*E*). The mean angles of the preferred phases (i.e. the circular means) were not significantly different between neuron groups (BZ neurons, $283.4 \pm 3.8°$; CZ neurons, $291.1 \pm 6.7°$; Watson–Williams *F*-test), but the distributions of the preferred phases of individual neurons differed ($P < 0.01$, Mardia-Watson-Wheeler test; Fig. 5*E*). This difference likely arose because the preferred phases of BZ neurons were more concentrated around the mean (group) angle when compared with those of CZ neurons, as reflected by their substantially longer group vector (BZ neurons, 0.90; CZ neurons, 0.61; Fig. 5*E*). These results indicate that although the average preferred spike phases of the populations of BZ and CZ neurons are the same with respect to cortical slow oscillations, the preferred phases of individual BZ neurons are comparatively more concentrated (i.e. more tightly locked) at the population level.

Because a thalamic LTS burst may be regarded as a singular event of special functional significance for target neurons in the cortex (Swadlow and Gusev 2001; Sherman 2001b; Sherman and Guillery 2011), we next tested whether these findings at the level of all spikes also held true for the onset of LTS bursts. When all neurons were analyzed (irrespective of the number of bursts each fired), the LTS bursts of BZ and CZ neurons ($n = 48$ and 80, respectively) were preferentially initiated at the ascending phase of cortical slow oscillations (Fig. 5*F*). Again, to qualify for the subsequent statistical analyses of phase preferences, a given neuron had to fire ≥40 LTS bursts during the 100 s recording. The first spikes of LTS bursts of nearly all the qualifying neurons were significantly locked to the slow oscillations (BZ, 31 of 31 qualifying neurons; CZ, 42 of 48 qualifying neurons; $P < 0.05$, Rayleigh's Uniformity Tests). In agreement with the analysis of all spikes, circular plots of the preferred phases of these individual phase-locked neurons confirmed their strong tendency to initiate LTS bursts during the ascending phase of the slow oscillations (Fig. 5*G*). The mean angles of the preferred phases of LTS bursts were not significantly different between neuron groups (BZ, $279.5 \pm 5.1°$; CZ, $282.3 \pm 6.4°$; Fig. 5*G*) and were not different to those for all spikes (Fig. 5*E*). However, unlike the firing of all spikes, the distribution of the preferred phases of LTS burst onsets of individual BZ neurons did not differ from that of individual CZ neurons and, indeed, the group vectors were similar in length (BZ neurons, 0.89; CZ neurons, 0.77; Fig. 5*G*). We also performed the same analyses for "non-LTS" spikes, that is, those not contained within defined LTS bursts (Supplementary Fig. 3*A–D*). For accurate circular statistics, we used a smaller sample of neurons (10 BZ and 10 CZ neurons), for which we had longer data files (duration of >350 s) containing >60 non-LTS spikes. In agreement with the analysis of all spikes and LTS burst onsets, there was a tendency for non-LTS spikes to be fired on the ascending phase of the slow oscillation, and the mean angles of the preferred phases of non-LTS spikes were similar between neuron groups (Supplementary Fig. 3*C,D*). The group vector for BZ neurons (0.88) was substantially longer than that for CZ neurons (0.62), indicating tighter locking by the BZ group.

The above analyses describe the phase-locking statistics across the 2 groups of neurons, but do not readily account for the cycle-to-cycle variation in the phase-locking of activity of individual neurons. To address this, we compared the vector lengths of all the LTS burst onsets and all the spikes of each neuron in the 2 zones. While individual BZ neurons tended to fire LTS bursts in a consistent manner from cycle to cycle, that is, they fired tightly around their mean phase angle, CZ neurons often fired at a wider range of angles, leading to large differences in the relative strength of phase-locked burst firing (Fig. 5*H*). Accordingly, the average vector length for LTS onsets of BZ neurons was significantly longer than that of CZ neurons (Fig. 5*I*). Vector lengths for the entire spike train were also significantly different (BZ, 0.69 ± 0.03; CZ, 0.47 ± 0.02; $P < 0.001$, Mann–Whitney *U*-test).

Given that ECoG power at slow oscillation frequencies was similar for BZ and CZ recordings (Fig. 5*A*), the distinct phase-locking properties of neurons in the 2 input zones were likely not the result of systematic differences in cortical activity. However, variation in the preferred phases of firing within each neuron group might be related to the locations of the recorded neurons within each zone of the motor thalamus. To address this possibility, we plotted the preferred phase vectors of all spikes of individual neurons according to the locations of their somata (Fig. 5*J*). The vectors of BZ neurons were relatively well aligned and were of a similar length, irrespective of their locations. In contrast, the vectors of CZ neurons were not so well aligned and varied substantially in length. However, there was no clear relationship between vector heterogeneity and location in CZ; for example, neurons with small vectors of one angle were essentially intermingled with neurons exhibiting large vectors of another angle (Fig. 5*J*). These distinct spatial distributions of preferred phase vectors further validate our parcellation of the motor thalamus into BZ and CZ.

In summary, the spike discharges of virtually all BZ and CZ neurons were phase-locked to ongoing cortical slow oscillations, and the 2 neuronal populations preferentially fired at the same (ascending) phase of the oscillation. However, the

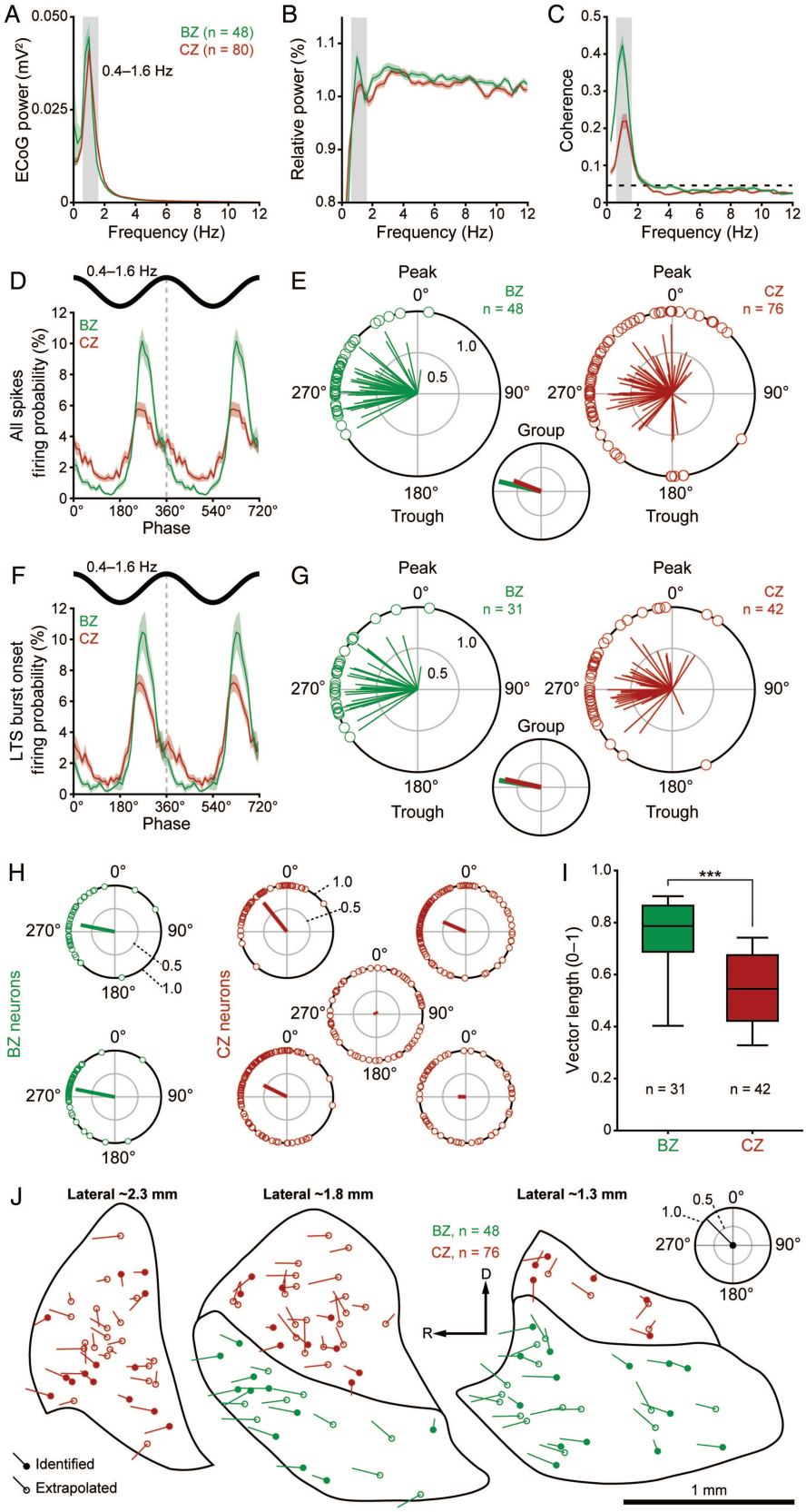

Figure 5. Spike timings of neurons in the BZ and CZ in relation to cortical slow oscillations (0.4–1.6 Hz). (*A*) Mean power spectra of ECoGs simultaneously recorded with all neurons in the BZ (green) and all neurons in the CZ (red). (*B*) Mean power spectra of the spike discharges of BZ neurons (green) and CZ neurons (red) relative to power at 0.25–50 Hz. Note the peaks in power at frequencies similar to those of the cortical slow oscillations. (*C*) Mean coherence spectra between ECoGs and all BZ neurons (green) or all CZ neurons (red). The dashed horizontal line denotes the 95% confidence level. Note that BZ neurons are more coherent with cortex. (*D*) Linear phase histograms of all spikes for all BZ neurons ($n = 48$, green) and all CZ neurons ($n = 80$, red). For clarity, 2 cortical slow oscillation cycles are shown. (*E*) Circular plots of phase-locked firing of BZ neurons

temporal coupling between cortex and single cell/population activity of BZ neurons was stronger and more precise than that between cortex and activity of CZ neurons.

Distinct Temporal Coupling of Neuronal Activity in the BZ and CZ with Cortical Spindle Oscillations

We next quantified the strength and distribution of phase-locked thalamic firing in relation to cortical spindle oscillations (7–12 Hz) in the frontal ECoG during SWA (Fig. 6). When the entire spike train of each neuron was analyzed, BZ neurons ($n = 48$) preferentially fired near the trough of the spindle oscillations, whereas CZ neurons ($n = 80$) appeared to fire earlier, that is, during the descending phase (Fig. 6*A*). We performed circular statistical analyses to further investigate this. To qualify for these analyses, a given neuron had to fire ≥40 spikes during "suprathreshold spindle periods" (see Materials and Methods), a first sampling criterion that helped ensure accurate determination of temporal coupling to robust spindle oscillations. When the entire spike train of each qualifying neuron was analyzed, most thalamic neurons were significantly phase-locked to the spindles (BZ, 34 of 42 qualifying neurons; CZ, 37 of 59 qualifying neurons; $P < 0.05$, Rayleigh's Uniformity Tests). Circular plots of the preferred phases of these individual phase-locked neurons reiterated the tendency for BZ and CZ neurons to fire at distinct phases of the spindle oscillations (Fig. 6*B*). Thus, unlike in the case of thalamic coupling to cortical slow oscillations, the mean angles of firing with respect to spindles were significantly different between neuron groups (BZ, 161.8 ± 7.4°; CZ, 140.1 ± 7.0°; $P < 0.05$, Watson-Williams *F*-test). In further contrast, the distributions of the preferred phases of individual neurons were not different (Mardia-Watson-Wheeler test) as reflected by group vectors of similar lengths (BZ neurons, 0.75; CZ neurons, 0.75; Fig. 6*B*). Moreover, the coherence between firing of BZ neurons and the ECoG was similar to that between firing of CZ neurons and the ECoG (data not shown).

We next tested whether these findings at the level of all spikes also held true for the onset of LTS bursts. For analysis of LTS bursts, we again had to use a smaller sample of neurons (10 BZ and 10 CZ neurons), for which we had long data files (duration of >350 s) that contained >150 LTS bursts. The first spikes of LTS bursts of nearly all the qualifying neurons were significantly locked to the spindle oscillations (BZ, 9 of 10 qualifying neurons; CZ, 9 of 10 qualifying neurons; $P < 0.05$, Rayleigh's Uniformity Tests). In agreement with the analysis of all spikes, the LTS bursts of BZ and CZ neurons were preferentially initiated at different phases of the spindle oscillations (Fig. 6*C*,*D*). The mean angles of the preferred phases of the LTS bursts of each neuron group were on the descending phase of the spindle oscillations, but the BZ neurons fired significantly later than CZ neurons (BZ, 160.0 ± 9.6°; CZ, 128.2 ± 13.3°; $P < 0.05$, Watson-Williams *F*-test). However, the distributions of the preferred phases of individual neurons and the group vector lengths (BZ neurons, 0.92; CZ neurons, 0.84; Fig. 6*D*) were similar for the 2 input zones. We also performed the same analyses for non-LTS spikes (Supplementary Fig. 3*E*,*F*). For the 2 small groups of qualifying neurons that were analyzed (7 BZ and 5 CZ neurons), there were no significant differences in their firing of non-LTS spikes. Thus, in contrast to the temporal coupling with slow oscillations, BZ and CZ neurons fired all spikes and LTS bursts at different phases of spindle oscillations, but there was no difference in the strength of their phase-locked firing.

We also examined the temporal relationships between all spikes fired by BZ or CZ neurons with higher-frequency ECoG oscillations during cortical activation (Supplementary Fig. 4). We focused our analyses on the characteristic ECoG oscillations at 15–50 Hz (Supplementary Fig. 4*A*). Power spectra of the spike trains of these thalamic neurons exhibited some minor features at 15–50 Hz (Supplementary Fig. 4*B*). However, on average, there was no significant coherence or consistent phase-locking between cortical and thalamic activities in this frequency band (Supplementary Fig. 4*C*), showing that temporal coupling of motor thalamic neuron discharges to cortical oscillations is most conspicuous at lower frequencies.

Spontaneous Activities of VA and VM Neurons are Similar

In this study, we focused our comparative analyses on the spontaneous activities of neurons in BZ (i.e. VA and VM nuclei) and CZ (i.e. VL nucleus), in part because these functionally distinct entities can be readily identified with contrasting GAD67 and VGluT2 immunoreactivities. The grouping together of VA and VM neurons into a single input zone appears warranted because any border between these 2 nuclei cannot be readily distinguished on the basis of cytoarchitecture or by markers for the axon terminals of their major afferents (Fig. 1*A–C* and Supplementary Fig. 1). However, as discussed (see Materials and Methods), the VM nucleus has long been regarded as separate from the VA (or the VA–VL complex) in rats and other species. In a final analysis, we tested whether the similar input organizations of VA and VM, as defined by uniformly abundant GAD67 immunolabeling, were reflected in constituent neurons with similar physiological properties (Fig. 7). Because the border between VA and VM is difficult to delineate precisely, we extracted a "virtual border" from a standard rat brain atlas (Paxinos and Watson 2007) and used it to divide the intensely GAD67-immunoreactive BZ accordingly. We were appropriately conservative in assigning recorded neurons to VA or VM; any neurons

(green) and CZ neurons (red). Vectors of preferred firing of individual neurons are shown as lines radiating from the center. Greater vector lengths indicate lower variance in the distribution around the mean phase angle. Each circle on the plot perimeter represents the preferred phase (i.e. mean phase of all the spikes) of an individual neuron. A mean vector for the preferred phases of neurons in each group is shown as a thick line (BZ in green, CZ in red) in the smaller circular plot. Note the longer group vector of BZ neurons. (*F* and *G*) As in *D* and *E*, but for only the first spike in each LTS burst ($n = 48$ BZ neurons and 80 CZ neurons in *F*). (*H*) Circular plots of onsets of the LTS bursts of 2 typical BZ neurons (green) and 5 typical CZ neurons (red) recorded in a single animal. Vector of preferred firing of each neuron is shown (radiating line), and each circle on the perimeter of each plot represents the phase of the first spike in each LTS burst fired by that single neuron. Note the firing of the CZ neurons was often relatively weak and dispersed in terms of phase-locking. (*I*) Vector lengths for the first spike in LTS bursts of BZ neurons (green) and CZ neurons (red). (*J*) Vectors of preferred firing for all spikes of individual BZ neurons (green) and CZ neurons (red) plotted against their somata locations on 3 parasagittal planes of the rat motor thalamus. Identified and extrapolated neurons are shown as filled and open circles, respectively. Phases and lengths of the vectors are scaled according to the key plot (top right). Gray boxes in *A–C* indicate the frequency range of slow oscillations analyzed. Data in *A–D* and *F* are mean ± SEM. *n*, the number of neurons/ECoGs analyzed. ***$P < 0.001$, Mann–Whitney *U*-test. R, rostral; D, dorsal.

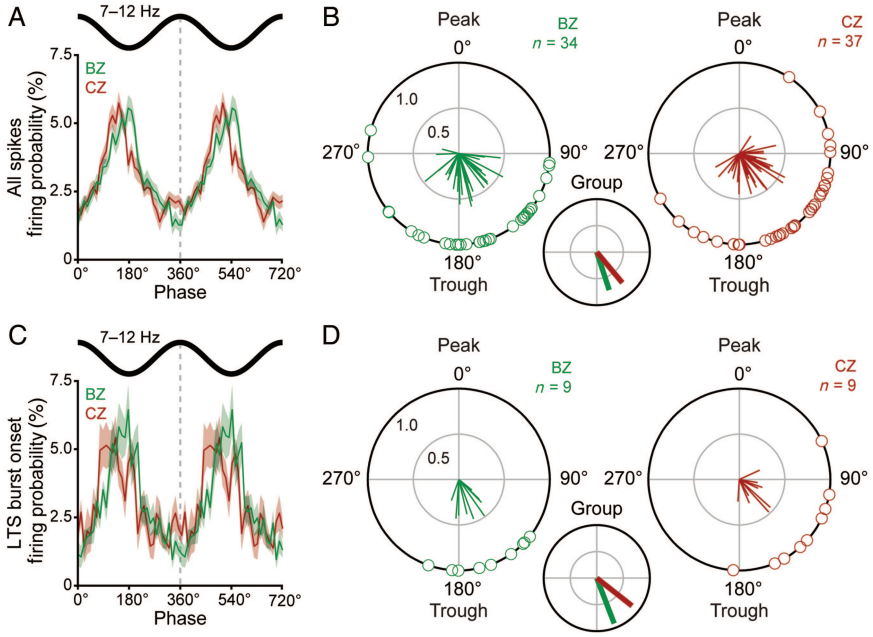

Figure 6. Spike timings of neurons in the BZ and CZ in relation to cortical spindle oscillations (7–12 Hz). (*A*) Linear phase histograms of all spikes for all neurons in the BZ ($n = 48$, green) and all neurons in the CZ ($n = 80$, red). For clarity, 2 spindle oscillation cycles are shown. (*B*) Circular plots of phase-locked firing of BZ neurons (green) and CZ neurons (red). Vectors of preferred firing of individual neurons are shown as lines radiating from the center. Greater vector lengths indicate lower variance in the distribution around the mean phase angle. Each circle on the plot perimeter represents the preferred phase (i.e. mean phase of all the spikes) of an individual neuron. A mean vector for the preferred phases of neurons in each group is shown as a thick line (BZ in green, CZ in red) in the smaller circular plot. Note the group vectors of BZ and CZ neurons are of similar length but different angles. (*C* and *D*) As in *A* and *B*, but for only the first spike in each LTS burst ($n = 10$ BZ neurons and 10 CZ neurons in *C*). Note the group vectors of BZ and CZ neurons are of similar lengths but different angles. Only neurons that fired ≥40 spikes (*B*) or LTS bursts (*D*) and were significantly phase-locked, were included in *B* and *D*. Data in *A* and *C* are mean ± SEM. *n*, the number of neurons analyzed.

within 200 μm of this virtual border were omitted from the comparative analyses (Fig. 7*A–D* and Table 1).

During SWA, VA and VM neurons showed no significant differences in their mean firing rates (Fig. 7*E*), their firing regularities (Fig. 7*F*), or their propensities to fire LTS bursts (Fig. 7*G*). The fine structure and other dynamics of LTS bursts fired by VA and VM neurons were also similar (Fig. 7*H–L*). This homogeneity in firing during SWA also held true for thalamic activity during cortical activation. Thus, the mean firing rates and firing regularities of VA and VM neurons were indistinguishable (Fig. 7*M*,*N*), and LTS bursts were similarly rare for neurons of both groups (Fig. 7*O*).

These electrophysiological data suggest that VA and VM neurons share the same essential functional properties and, when taken together with our anatomical findings, serve to reinforce the notion that VA and VM neurons collectively make up a single, elementary component of forebrain circuits, that is, the BZ of motor thalamus.

Discussion

Here, we have parcellated the motor thalamus into BZ and CZ, and shown for the first time that, regardless of brain state, identified neurons precisely localized to the BZ and CZ have indistinguishable firing rates. Moreover, we show that the definitive differences in subcortical GABAergic and glutamatergic inputs to these motor thalamic neurons are better reflected in their distinct firing patterns, and particularly, their temporal coupling to low-frequency oscillations in the motor cortex.

Firing Rates of Thalamic Neurons in the 2 Input Zones are Similar

Basal ganglia output nuclei give rise to the large GABAergic (GAD67+) axon terminals that densely distribute within VA and VM, whereas cerebellar nuclei are the origin of the large/giant glutamatergic (VGluT2+) axon terminals that are confined to VL (Kuramoto et al. 2011). Accordingly, these 2 subcortical afferents define largely non-overlapping zones in the rat thalamus (Deniau et al. 1992; Kuramoto et al. 2011). Delineation of a BZ (i.e. VA and VM nuclei) and a CZ (i.e. VL nucleus) according to these axon terminal markers thus affords functionally relevant insights into distinct routes of information flow, while circumventing ambiguities arising from assessing cytoarchitecture or markers of other major inputs of the motor thalamus. This delineation is particularly important for rodent motor thalamus. Cytoarchitecture is more informative in cats and monkeys (Jones 2007), though it probably cannot fully segregate BZ and CZ (Percheron et al. 1996; Calzavara et al. 2005; Kultas-Ilinsky et al. 2011).

The synapses established between the large axon terminals of nigrothalamic or cerebellothalamic afferents and the proximal dendrites or somata of their target neurons often contain multiple release sites (Aumann et al. 1994; Aumann and Horne 1996; Bodor et al. 2008). Such specialized synaptic arrangements in the thalamus are commonly associated with powerful, high-fidelity synaptic transmission (Sherman and Guillery 2006). Moreover, output neurons of the basal ganglia and cerebellar nuclei are well known to fire tonically and at high rates (>25 spikes/s) under "resting conditions," irrespective of anesthesia, brain state, or species (Thach 1968; DeLong 1971; DeLong et al. 1983; Chiken and Tokuno 2003;

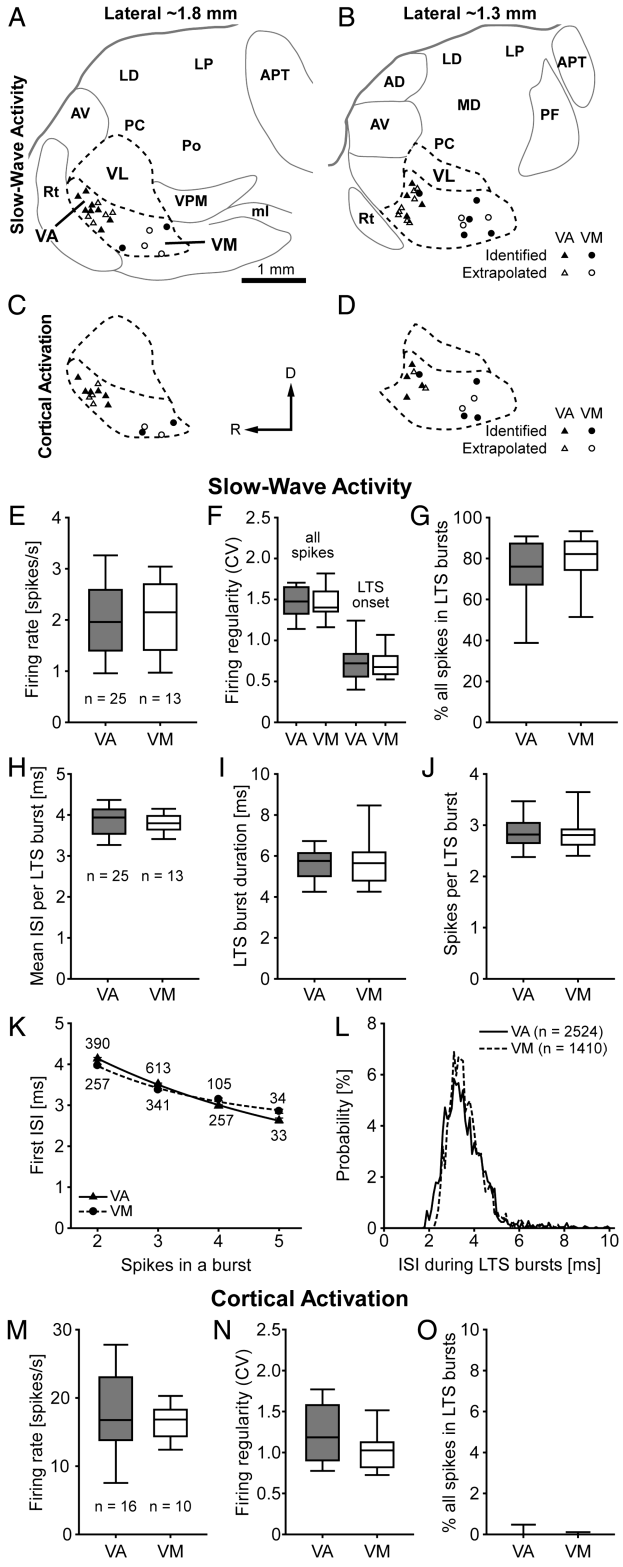

Figure 7. Quantitative comparisons of the activities of VA and VM neurons. (*A–D*) Parasagittal views of the rat motor thalamus at 2 different mediolateral planes, ~1.8 mm (*A* and *C*) and ~1.3 mm (*B* and *D*) lateral to Bregma, showing the locations of all VA and VM neurons recorded during either SWA (*A* and *B*) or cortical activation (*C* and *D*). Neurons located near the "virtual border" between VA and VM were not analyzed (see Results). (*E–G*) Mean firing rates (*E*), firing regularities separately defined for all spikes and for the onset times of LTS bursts (*F*), and mean percentage of all spikes occurring in LTS bursts (*G*) during SWA. Note similarities between VA and VM neurons. (*H–J*) Mean ISI per LTS burst (*H*), mean burst duration (*I*), and mean number of spikes per burst (*J*). Note that VA and VM neurons fire similar LTS bursts. (*K*) The duration, and highly predictive nature, of the first ISI in a given LTS burst were similar for VA and VM neurons ($R^2 > 0.99$ for both exponential decay curves). (*L*) Normalized ISI histograms (0.1 ms bins) for all spikes in all LTS bursts. Note the unimodal distributions for VA and VM neurons almost entirely overlapped. (*M–O*) Mean firing rates (*M*), firing regularities (*N*), and mean percentage of all spikes in LTS bursts (*O*) during cortical activation. Note similarities between VA and VM neurons. Scale bar in *A* also applies to *B–D*. Data in *K* are mean ± SEM. *n*, the number of recorded neurons (*E–J* and *M–O*), the number of LTS bursts (*K*), or the number of ISIs (*L*). Abbreviations are listed in Figures 1 and 2.

Magill et al. 2004; Rowland and Jaeger 2005; Baron et al. 2011; Blenkinsop and Lang 2011). Presumably then, neurons in BZ are almost continuously bombarded by powerful GABAergic inputs, whereas neurons in CZ are bombarded by efficacious glutamatergic inputs, even in the absence of purposeful movement. This should result in an inhibitory–excitatory "imbalance" across the 2 zones much of the time, the net result of which being relatively less active BZ neurons. Our results, based on anatomically verified neurons recorded during controlled brain states, argue against this prediction. The mean rates and brain state dependency of the firing of neurons in BZ and CZ were matched during SWA or cortical activation. This finding likely extends beyond anesthesia or rodents. Indeed, the spontaneous firing rates of rat motor thalamic neurons during cortical activation in the present study tally with those of motor thalamic neurons in alert monkeys at rest (Anderson and Turner 1991; Vitek et al. 1994; Pessiglione et al. 2005). The same finding also helps explain why thalamic neurons recorded in areas receiving basal ganglia or cerebellar inputs (as indirectly defined) in monkeys and humans during different behaviors and vigilance states have similar firing rates (Anderson and Turner 1991; Ohara et al. 2007).

Our findings help refine an influential scheme that classifies thalamic afferents as either "drivers," which carry the key information to be relayed to cortex, or "modulators" (Sherman and Guillery 2006). It has been proposed that CZ receives a driver input from cerebellar nuclei, whereas BZ lacks subcortical glutamatergic driver inputs but instead receives drivers from neocortical layer 5 (Sherman and Guillery 2006). By definition, information-bearing drivers are not necessarily the primary cause of spontaneous activity in their thalamic targets (Sherman and Guillery 2006). Nevertheless, an important implication of our data is that the supposedly powerful impact of highly active subcortical driver inputs is not readily translated to higher spontaneous firing rates, at least in CZ. So how can thalamic neurons in the 2 zones discharge at equivalent rates despite apparently imbalanced inhibitory–excitatory inputs? The paradoxically poor translation of bombardment by glutamatergic cerebellar inputs into higher net activity in CZ (when compared with BZ) could be related to the high probability of neurotransmitter release and paired-pulse depression that are typical of drivers (Sherman and Guillery 2006). We speculate that the high-frequency sustained firing of cerebellar nuclei neurons in vivo could result in a profound depression of their synapses, in turn placing special emphasis on the renewal of spiking after the pauses that occasionally punctuate their tonic activity (De Zeeuw et al. 2011). Moreover, even without short-term depression, conductances at synapses formed by cerebellar, and basal ganglia axons could be much smaller than predicted, perhaps supported by tailored homeostatic plasticity (Pozo and Goda 2010).

Alternatively, or additionally, other inputs to BZ or CZ neurons could counterbalance their basal ganglia- and cerebellar-derived inputs. Our qualitative analyses suggest that the distributions of glutamatergic cortical inputs, cholinergic inputs, and presumed GABAergic Rt inputs are similar across the 2 zones (Supplementary Fig. 1), thus offering no clear structural substrate for neutralizing the apparent inhibitory–excitatory imbalance therein. That said, we did not explore the ultrastructural substrates or physiological impact of these other afferents, so we cannot rule out the possibility they are important for counterbalancing thalamic activity. Indeed, a possible driver input from cortical layer 5 to BZ neurons (Sherman and Guillery 2006) could offset the barrage of GABAergic inputs from the basal ganglia. However, the paucity of large VGluT1+ axon terminals in BZ suggests that such cortical drivers are rare and/or that they lack the typical driver terminal structure.

Temporal Coupling to Cortical Rhythms Discriminates Motor Thalamic Neurons

Neurons of BZ and CZ had similar propensities to fire LTS bursts. An intrinsic *T*-type Ca^{2+} current, I_T, is critical for thalamic LTS burst firing; greater membrane potential hyperpolarization for longer durations produces larger I_T and thence, faster bursts containing more action potentials (Huguenard 1996; Tscherter et al. 2011). Again, one would predict that neurons in BZ are more hyperpolarized than those in CZ. Our extracellular recordings demonstrate that any such membrane potential difference is insufficient to manifest as differences in the firing rate or propensity to fire LTS bursts, in line with findings in humans (Ohara et al. 2007). However, BZ neurons fire slower LTS bursts than CZ neurons, but with the same number of action potentials, suggesting they have different intrinsic membrane properties. This distinction is not readily explained by cell type-specific diversity in I_T alone (Tscherter et al. 2011).

As in sleeping or anesthetized rats, cats, and humans (Steriade 2000, 2006), cortical activity during SWA was dominated by a slow oscillation (~1 Hz) that is generated through synchronous membrane potential transitions of pyramidal neurons (Steriade, Nuñez, et al. 1993; Contreras and Steriade 1995). The resultant synchronized activity in corticofugal pathways may entrain thalamic activity (Steriade, Contreras, et al. 1993; Contreras and Steriade 1995) and, indeed, the spikes and LTS burst onsets of BZ and CZ neurons were timed with cortical slow oscillations. Both groups of neurons preferentially fired at the same early ascending phase of the slow oscillation, a transition that is likely led by layer 5/6 pyramidal neurons that, in turn, presumably excite thalamic neurons at short delays (Sakata and Harris 2009; Chauvette et al. 2010). However, the firing of neurons across BZ was stronger and more precisely coupled to the slow oscillations. This distinction could arise from the different types of cortical inputs to the 2 zones; the proposed driver inputs to BZ neurons (Sherman and Guillery 2006), even if they are relatively sparse or lack the typically large terminal structure, could be more effective at timing/synchronizing their activity. Because neurons in the substantia nigra pars reticulata exhibit only subtle or no modulations of firing in time with cortical slow oscillations (Magill et al. 2004), their output is likely not responsible for the exquisite phase-locking of BZ neurons. However, cerebellar nuclear neurons can engage in more phasic firing during SWA (Rowland et al. 2010) and thus, they could interfere with or otherwise influence the entrainment of CZ neurons. The slow oscillation is likely of cortical origin (Chauvette et al. 2010), and it is unclear whether thalamocortical neurons can initiate active cortical states. However, this does not preclude other roles for thalamocortical inputs in shaping cortical neuron activity during slow oscillations. It is well established that VM neurons project to layer 1 of frontal cortical areas (Herkenham 1979; Arbuthnott et al. 1990; Desbois and Villanueva 2001; Mitchell and Cauller 2001; Rubio-Garrido et al. 2007, 2009). Importantly, VA neurons, but not VL neurons, also densely innervate layer 1 over wide areas (Kuramoto et al. 2009). The specialized cortical innervation by BZ neurons, together with their highly synchronized "early phase" firing as a population, suggests their outputs (and particularly those captured in LTS bursts) are well suited to rhythmically coordinate, in a widespread manner, the activities of the many cortical interneurons and pyramidal neurons that extend their dendrites into layer 1.

Importantly, we show that the discriminating features of BZ and CZ coupling to slow oscillations do not apply to all ECoG rhythms. Thus, BZ and CZ neurons fire at different phases of spindle oscillations, but the strengths of their phase-locked firing are similar. Given that spindle oscillations in the cortex and thalamic relay nuclei are critically dependent on Rt (Pinault 2004), and that Rt inputs to both zones are structurally similar, these different preferred phases might arise from temporal delays in the spindles produced across neighboring sectors of Rt that innervate BZ or CZ (Pinault and Deschênes 1998). The difference in the preferred phases of the firing of BZ and CZ neurons during spindles compared with slow oscillations may reflect differences in the initiators of these network oscillations; Rt is the major pacemaker of spindle activity, whereas the neocortex likely initiates slow oscillations (Fuentealba and Steriade 2005). It is also possible that the precise features of temporal coupling might vary according to the (frontal) cortical area examined.

Additional Functional Considerations

Defining the spatiotemporal organization of spontaneous activity in different motor thalamic regions at rest, with respect to ongoing cortical activity, provides a vital context for understanding the neural basis of voluntary movement. In recognizing the importance of directly correlating the structure (input organization) of motor thalamus with its function, we show that the activities of thalamic projection neurons in identified BZ and CZ are surprisingly alike in some respects, but different in others. Because our experimental strategy required general anesthesia (physical stability is paramount for juxtacellular recording/labeling), we could not directly investigate neuronal correlates of behavior. The recording of individual, precisely localized BZ and CZ neurons has not yet been achieved during movement, although this may eventually be possible in awake, head-restrained animals (Isomura et al. 2009). Despite the caveats of our strategy, it enabled robust sampling of identified neurons that in turn allowed us to define a wide range of activities according to the cell type and brain state, to infer intrinsic properties, and to address the predicted activity differences across the 2 input zones. In the future, it would be important to test the validity of our

findings in behaving animals. Thus, although it is currently unclear how, during purposeful action, the concerted efforts of basal ganglia and cerebellar output neurons impact on the firing rates of thalamocortical neurons in rigorously defined input zones, equivalent firing rates during rest might well extend to certain movements (Anderson and Turner 1991). Despite similar firing rates, BZ and CZ neurons surely subserve distinct functions during rest or movement. Indeed, complementing their distinct inputs, BZ neurons (but not CZ neurons) provide a widespread and dense innervation of cortical layer 1, allowing for coincident excitation of many cortical neurons through their distal dendrites. Our data further highlight the potential importance of firing patterns and suggest that "temporal coding" through oscillatory synchronization is another key way in which the outputs of BZ and CZ neurons are distinguishable in their cortical targets, thereby perhaps partly underlying the different roles of basal ganglia and cerebellum in behavior.

Supplementary Material

Supplementary material can be found at: http://www.cercor.oxfordjournals.org/

Funding

This work was supported by the Medical Research Council UK (award U138197109) and Parkinson's UK (grant number G-0806). K.C.N. is supported by a Long-Term Fellowship of the Human Frontier Science Program (LT000396/2009-L). A.S. was also supported by a Marie Curie European Re-integration Grant (SNAP-PD) awarded by the European Union. Funding to pay the Open Access publication charges for this article was provided by Medical Research Council UK (award U138197109).

Notes

We are grateful to Drs R.W. Guillery, N. Mallet, P. Dodson, D. Kase, and E. Kuramoto for valuable scientific discussions and to Dr T. Kaneko for antibodies to VGluTs. We also thank E. Norman, K. Whitworth, and G. Hazell for expert technical assistance. *Conflict of Interest*: None declared.

References

Anderson ME, Turner RS. 1991. Activity of neurons in cerebellar-receiving and pallidal-receiving areas of the thalamus of the behaving monkey. J Neurophysiol. 66:879–893.

Arai R, Jacobowitz DM, Deura S. 1994. Distribution of calretinin, calbindin-D28k, and parvalbumin in the rat thalamus. Brain Res Bull. 33:595–614.

Arbuthnott GW, MacLeod NK, Maxwell DJ, Wright AK. 1990. Distribution and synaptic contacts of the cortical terminals arising from neurons in the rat ventromedial thalamic nucleus. Neuroscience. 38:47–60.

Aumann TD, Horne MK. 1996. A comparison of the ultrastructure of synapses in the cerebello-rubral and cerebello-thalamic pathways in the rat. Neurosci Lett. 211:175–178.

Aumann TD, Rawson JA, Finkelstein DI, Horne MK. 1994. Projections from the lateral and interposed cerebellar nuclei to the thalamus of the rat: a light and electron microscopic study using single and double anterograde labelling. J Comp Neurol. 349:165–181.

Baron MS, Chaniary KD, Rice AC, Shapiro SM. 2011. Multi-neuronal recordings in the basal ganglia in normal and dystonic rats. Front Syst Neurosci. 5:67.

Berens P. 2009. CircStat: a MATLAB toolbox for circular statistics. J Statistical Software. 31:1–21.

Blenkinsop TA, Lang EJ. 2011. Synaptic action of the olivocerebellar system on cerebellar nuclear spike activity. J Neurosci. 31:14708–14720.

Bodor ÁL, Giber K, Rovó Z, Ulbert I, Acsády L. 2008. Structural correlates of efficient GABAergic transmission in the basal ganglia-thalamus pathway. J Neurosci. 28:3090–3102.

Brecht M, Krauss A, Muhammad S, Sinai-Esfahani L, Bellanca S, Margrie TW. 2004. Organization of rat vibrissa motor cortex and adjacent areas according to cytoarchitectonics, microstimulation, and intracellular stimulation of identified cells. J Comp Neurol. 479:360–373.

Calzavara R, Zappalà A, Rozzi S, Matelli M, Luppino G. 2005. Neurochemical characterization of the cerebellar-recipient motor thalamic territory in the macaque monkey. Eur J Neurosci. 21:1869–1894.

Chauvette S, Crochet S, Volgushev M, Timofeev I. 2011. Properties of slow oscillation during slow-wave sleep and anesthesia in cats. J Neurosci. 31:14998–15008.

Chauvette S, Volgushev M, Timofeev I. 2010. Origin of active states in local neocortical networks during slow sleep oscillation. Cereb Cortex. 20:2660–2674.

Chiken S, Tokuno H. 2003. Ablation of striatal interneurons influences activities of entopeduncular neurons. Neuroreport. 14:675–678.

Contreras D, Steriade M. 1995. Cellular basis of EEG slow rhythms: a study of dynamic corticothalamic relationships. J Neurosci. 15:604–622.

DeLong MR. 1971. Activity of pallidal neurons during movement. J Neurophysiol. 34:414–427.

DeLong MR, Crutcher MD, Georgopoulos AP. 1983. Relations between movement and single cell discharge in the substantia nigra of the behaving monkey. J Neurosci. 3:1599–1606.

Deniau JM, Kita H, Kitai ST. 1992. Patterns of termination of cerebellar and basal ganglia efferents in the rat thalamus. Strictly segregated and partly overlapping projections. Neurosci Lett. 144:202–206.

Desbois C, Villanueva L. 2001. The organization of lateral ventromedial thalamic connections in the rat: a link for the distribution of nociceptive signals to widespread cortical regions. Neuroscience. 102:885–898.

De Zeeuw CI, Hoebeek FE, Bosman LWJ, Schonewille M, Witter L, Koekkoek SK. 2011. Spatiotemporal firing patterns in the cerebellum. Nat Rev Neurosci. 12:327–344.

Domich L, Oakson G, Steriade M. 1986. Thalamic burst patterns in the naturally sleeping cat: a comparison between cortically projecting and reticularis neurones. J Physiol (Lond). 379:429–449.

Donoghue JP, Wise SP. 1982. The motor cortex of the rat: cytoarchitecture and microstimulation mapping. J Comp Neurol. 212:76–88.

Fanselow EE, Sameshima K, Baccala LA, Nicolelis MA. 2001. Thalamic bursting in rats during different awake behavioral states. Proc Natl Acad Sci USA. 98:15330–15335.

Fuentealba P, Steriade M. 2005. The reticular nucleus revisited: intrinsic and network properties of a thalamic pacemaker. Prog Neurobiol. 75:125–141.

Fujiyama F, Furuta T, Kaneko T. 2001. Immunocytochemical localization of candidates for vesicular glutamate transporters in the rat cerebral cortex. J Comp Neurol. 435:379–387.

Groenewegen HJ, Witter MP. 2004. Thalamus. In: Paxinos G, editor. The rat nervous system. 3rd ed. San Diego (CA): Elsevier Academic Press. p. 407–453.

Herkenham M. 1979. The afferent and efferent connections of the ventromedial thalamic nucleus in the rat. J Comp Neurol. 183:487–517.

Hioki H, Fujiyama F, Taki K, Tomioka R, Furuta T, Tamamaki N, Kaneko T. 2003. Differential distribution of vesicular glutamate transporters in the rat cerebellar cortex. Neuroscience. 117:1–6.

Huguenard JR. 1996. Low-threshold calcium currents in central nervous system neurons. Annu Rev Physiol. 58:329–348.
Ilinsky IA, Kultas-Ilinsky K. 1987. Sagittal cytoarchitectonic maps of the *Macaca mulatta* thalamus with a revised nomenclature of the motor-related nuclei validated by observations on their connectivity. J Comp Neurol. 262:331–364.
Ilinsky IA, Kultas-Ilinsky K. 2002. Stereotactic atlas of the *Macaca mulatta* thalamus and adjacent basal ganglia nuclei. New York (NY): Kulwar Academic/Plenum Publishers.
Isomura Y, Harukuni R, Takekawa T, Aizawa H, Fukai T. 2009. Microcircuitry coordination of cortical motor information in self-initiation of voluntary movements. Nat Neurosci. 12:1586–1593.
Jeanmonod D, Magnin M, Morel A. 1996. Low-threshold calcium spike bursts in the human thalamus. Common physiopathology for sensory, motor and limbic positive symptoms. Brain. 119(Pt 2):363–375.
Johnson DH. 1996. Point process models of single-neuron discharges. J Comput Neurosci. 3:275–299.
Jones EG. 2007. The thalamus. 2nd ed. Cambridge (UK): Cambridge University Press.
Kincaid AE, Wilson CJ. 1996. Corticostriatal innervation of the patch and matrix in the rat neostriatum. J Comp Neurol. 374:578–592.
Kultas-Ilinsky K, Ilinsky IA, Verney C. 2011. Glutamic acid decarboxylase isoform 65 immunoreactivity in the motor thalamus of humans and monkeys: γ-aminobutyric acidergic connections and nuclear delineations. J Comp Neurol. 519:2811–2837.
Kuramoto E, Fujiyama F, Nakamura KC, Tanaka Y, Hioki H, Kaneko T. 2011. Complementary distribution of glutamatergic cerebellar and GABAergic basal ganglia afferents to the rat motor thalamic nuclei. Eur J Neurosci. 33:95–109.
Kuramoto E, Furuta T, Nakamura KC, Unzai T, Hioki H, Kaneko T. 2009. Two types of thalamocortical projections from the motor thalamic nuclei of the rat: a single neuron-tracing study using viral vectors. Cereb Cortex. 19:2065–2077.
Lacey CJ, Bolam JP, Magill PJ. 2007. Novel and distinct operational principles of intralaminar thalamic neurons and their striatal projections. J Neurosci. 27:4374–4384.
Lachaux JP, Rodriguez E, Martinerie J, Varela FJ. 1999. Measuring phase synchrony in brain signals. Hum Brain Mapp. 8:194–208.
Le Van Quyen M, Foucher J, Lachaux J, Rodriguez E, Lutz A, Martinerie J, Varela FJ. 2001. Comparison of Hilbert transform and wavelet methods for the analysis of neuronal synchrony. J Neurosci Methods. 111:83–98.
Llinás RR, Steriade M. 2006. Bursting of thalamic neurons and states of vigilance. J Neurophysiol. 95:3297–3308.
Lu SM, Guido W, Sherman SM. 1992. Effects of membrane voltage on receptive field properties of lateral geniculate neurons in the cat: contributions of the low-threshold Ca^{2+} conductance. J Neurophysiol. 68:2185–2198.
Magill PJ, Bolam JP, Bevan MD. 2001. Dopamine regulates the impact of the cerebral cortex on the subthalamic nucleus-globus pallidus network. Neuroscience. 106:313–330.
Magill PJ, Bolam JP, Bevan MD. 2000. Relationship of activity in the subthalamic nucleus-globus pallidus network to cortical electroencephalogram. J Neurosci. 20:820–833.
Magill PJ, Pogosyan A, Sharott A, Csicsvari J, Bolam JP, Brown P. 2006. Changes in functional connectivity within the rat striatopallidal axis during global brain activation in vivo. J Neurosci. 26:6318–6329.
Magill PJ, Sharott A, Bolam JP, Brown P. 2004. Brain state-dependency of coherent oscillatory activity in the cerebral cortex and basal ganglia of the rat. J Neurophysiol. 92:2122–2136.
Mallet N, Pogosyan A, Márton LF, Bolam JP, Brown P, Magill PJ. 2008. Parkinsonian beta oscillations in the external globus pallidus and their relationship with subthalamic nucleus activity. J Neurosci. 28:14245–14258.
Mitchell BD, Cauller LJ. 2001. Corticocortical and thalamocortical projections to layer I of the frontal neocortex in rats. Brain Res. 921:68–77.
Nambu A. 2008. Seven problems on the basal ganglia. Curr Opin Neurobiol. 18:595–604.
Ohara S, Taghva A, Kim JH, Lenz FA. 2007. Spontaneous low threshold spike bursting in awake humans is different in different lateral thalamic nuclei. Exp Brain Res. 180:281–288.
Paxinos G, Watson C. 2007. The rat brain in stereotaxic coordinates. 6th ed. Amsterdam (Netherland), Boston (MA): Academic Press.
Percheron G, François C, Talbi B, Yelnik J, Fénelon G. 1996. The primate motor thalamus. Brain Res Rev. 22:93–181.
Pessiglione M, Guehl D, Rolland A-S, François C, Hirsch EC, Féger J, Tremblay L. 2005. Thalamic neuronal activity in dopamine-depleted primates: evidence for a loss of functional segregation within basal ganglia circuits. J Neurosci. 25:1523–1531.
Pinault D. 1996. A novel single-cell staining procedure performed in vivo under electrophysiological control: morpho-functional features of juxtacellularly labeled thalamic cells and other central neurons with biocytin or Neurobiotin. J Neurosci Methods. 65:113–136.
Pinault D. 2004. The thalamic reticular nucleus: structure, function and concept. Brain Res Rev. 46:1–31.
Pinault D, Deschênes M. 1998. Projection and innervation patterns of individual thalamic reticular axons in the thalamus of the adult rat: a three-dimensional, graphic, and morphometric analysis. J Comp Neurol. 391:180–203.
Pozo K, Goda Y. 2010. Unraveling mechanisms of homeostatic synaptic plasticity. Neuron. 66:337–351.
Ramcharan EJ, Gnadt JW, Sherman SM. 2005. Higher-order thalamic relays burst more than first-order relays. Proc Natl Acad Sci USA. 102:12236–12241.
Rowland NC, Goldberg JA, Jaeger D. 2010. Cortico-cerebellar coherence and causal connectivity during slow-wave activity. Neuroscience. 166:698–711.
Rowland NC, Jaeger D. 2005. Coding of tactile response properties in the rat deep cerebellar nuclei. J Neurophysiol. 94:1236–1251.
Rubio-Garrido P, Pérez-de-Manzo F, Clascá F. 2007. Calcium-binding proteins as markers of layer-I projecting vs. deep layer-projecting thalamocortical neurons: a double-labeling analysis in the rat. Neuroscience. 149:242–250.
Rubio-Garrido P, Pérez-de-Manzo F, Porrero C, Galazo MJ, Clascá F. 2009. Thalamic input to distal apical dendrites in neocortical layer 1 is massive and highly convergent. Cereb Cortex. 19:2380–2395.
Sakai ST, Grofovà I. 2003. Distribution of the basal ganglia and cerebellar projections to the rodent motor thalamus. In: Graybiel AM, DeLong MR, Kitai ST, editors. The basal ganglia VI. New York (NY): Plenum Publishers. p. 455–462.
Sakata S, Harris KD. 2009. Laminar structure of spontaneous and sensory-evoked population activity in auditory cortex. Neuron. 64:404–418.
Sharott A, Doig NM, Mallet N, Magill PJ. 2012. Relationships between the firing of identified striatal interneurons and spontaneous and driven cortical activities in vivo. J Neurosci. 32:13221–13236.
Sherman SM. 2001a. Tonic and burst firing: dual modes of thalamocortical relay. Trends Neurosci. 24:122–126.
Sherman SM. 2001b. A wake-up call from the thalamus. Nat Neurosci. 4:344–346.
Sherman SM, Guillery RW. 2011. Distinct functions for direct and transthalamic corticocortical connections. J Neurophysiol. 106: 1068–1077.
Sherman SM, Guillery R. 2006. Exploring the thalamus and its role in cortical function. 2nd ed. Cambridge (MA): MIT Press.
Siapas AG, Lubenov EV, Wilson MA. 2005. Prefrontal phase locking to hippocampal theta oscillations. Neuron. 46:141–151.
Slézia A, Hangya B, Ulbert I, Acsády L. 2011. Phase advancement and nucleus-specific timing of thalamocortical activity during slow cortical oscillation. J Neurosci. 31:607–617.
Steriade M. 2000. Corticothalamic resonance, states of vigilance and mentation. Neuroscience. 101:243–276.

Steriade M. 2006. Grouping of brain rhythms in corticothalamic systems. Neuroscience. 137:1087–1106.
Steriade M, Contreras D, Curró Dossi R, Nuñez A. 1993. The slow (<1 Hz) oscillation in reticular thalamic and thalamocortical neurons: scenario of sleep rhythm generation in interacting thalamic and neocortical networks. J Neurosci. 13:3284–3299.
Steriade M, Nuñez A, Amzica F. 1993. A novel slow (<1 Hz) oscillation of neocortical neurons in vivo: depolarizing and hyperpolarizing components. J Neurosci. 13:3252–3265.
Swadlow HA, Gusev AG. 2001. The impact of 'bursting' thalamic impulses at a neocortical synapse. Nat Neurosci. 4:402–408.
Thach WT. 1968. Discharge of Purkinje and cerebellar nuclear neurons during rapidly alternating arm movements in the monkey. J Neurophysiol. 31:785–797.
Tlamsa AP, Brumberg JC. 2010. Organization and morphology of thalamocortical neurons of mouse ventral lateral thalamus. Somatosens Mot Res. 27:34–43.
Tscherter A, David F, Ivanova T, Deleuze C, Renger JJ, Uebele VN, Shin H-S, Bal T, Leresche N, Lambert RC. 2011. Minimal alterations in T-type calcium channel gating markedly modify physiological firing dynamics. J Physiol (Lond). 589:1707–1724.
Vitek JL, Ashe J, DeLong MR, Alexander GE. 1994. Physiologic properties and somatotopic organization of the primate motor thalamus. J Neurophysiol. 71:1498–1513.
Yamamoto T, Noda T, Miyata M, Nishimura Y. 1984. Electrophysiological and morphological studies on thalamic neurons receiving entopedunculo- and cerebello-thalamic projections in the cat. Brain Res. 301:231–242.

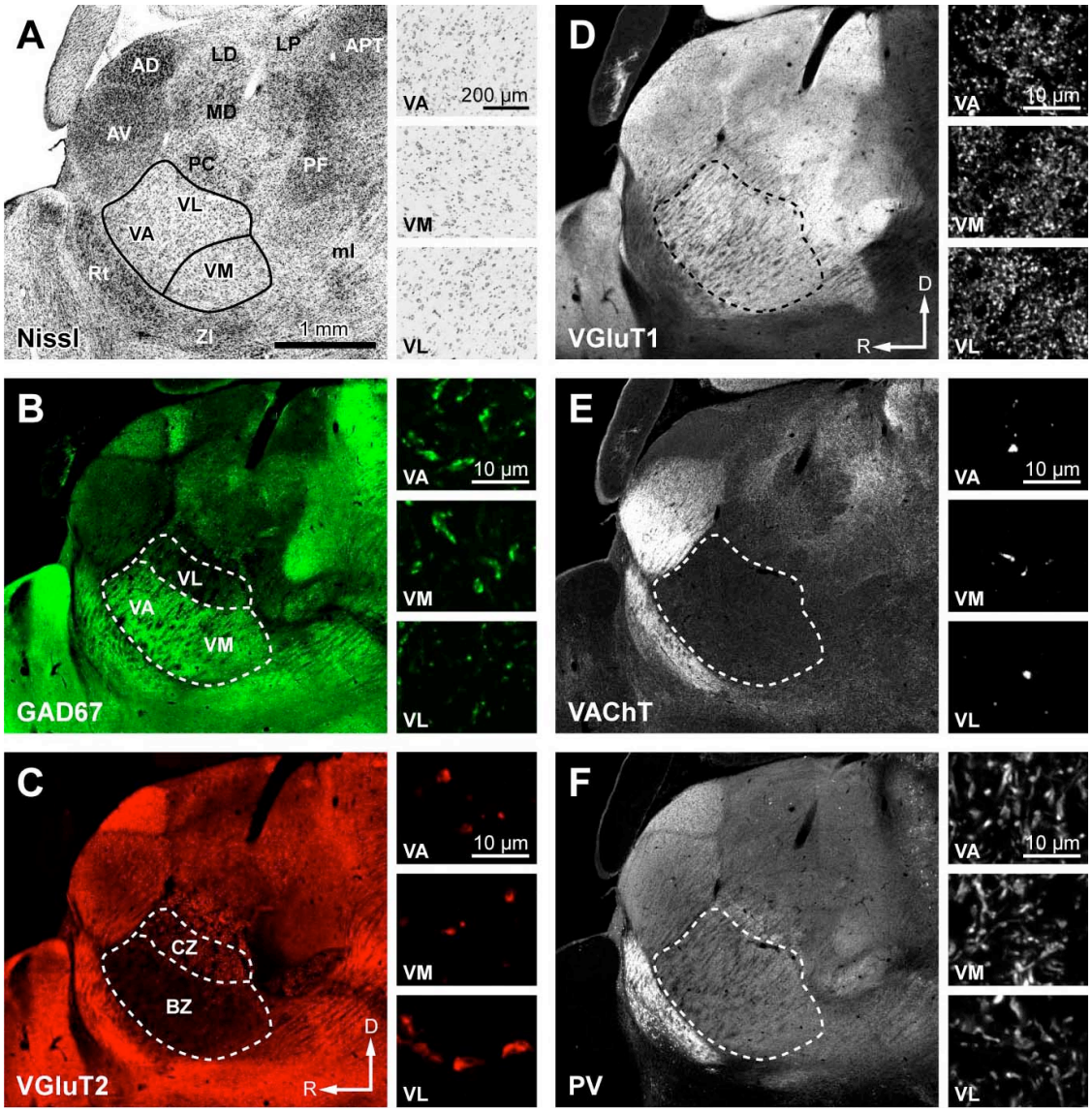

Supplementary Figure 1. Distributions of GAD67 and VGluT2, but not other axon terminal markers, delineate basal ganglia-recipient and cerebellar-recipient zones of rat motor thalamus. Matched fluorescence images of Nissl labeling (*A*; inverted tone) and immunoreactivities for GAD67 (*B*), VGluT2 (*C*), VGluT1 (*D*), VAChT (*E*), and PV (*F*) at the level of motor thalamus (VA, VM and VL nuclei). *A*, *E*, *F* are from the same parasagittal section, *B–D* are from an immediately adjacent section. (*A*) 'Standard' cytoarchitectonic borders of VM and VA-VL complex (black line) were extrapolated from an atlas (Paxinos and Watson 2007; ~1.5 mm lateral from Bregma). These nuclei have

similar cytoarchitecture (*insets*). (*B*, *C*) GAD67 and VGluT2 immunoreactivities do not respect these cytoarchitectonic boundaries but do show complementary patterns in the motor thalamus; GAD67 is more intense ventrally (*B*), whereas VGluT2 is more evident dorsally (*C*). (*D–F*) VGluT1, VAChT and PV are homogeneously distributed across the motor thalamus. Thus, a basal ganglia-recipient zone (BZ), corresponding to VA and VM, is delineated by GAD67 immunoreactivity, whereas a cerebellar-recipient zone (CZ), corresponding to VL, by VGluT2 immunoreactivity (borders indicated with dashed lines in *B* and *C*). (*B–F insets*) High-magnification confocal images of immunoreactivity in VA, VM and VL. GAD67-immunoreactive punctate profiles are larger and more dense in VA and VM compared to VL (*B*), whereas VGluT2-immunoreactive puncta are much larger and more dense in VL compared to VA and VM (*C*). Note the paucity of similarly large VGluT1+ axon terminals in BZ and CZ (*D insets*). Abbreviations are defined in Figures 1 and 2. Scale bar in *A* also applies to low-magnification images in *B–F*. The three insets in each panel share the same scale.

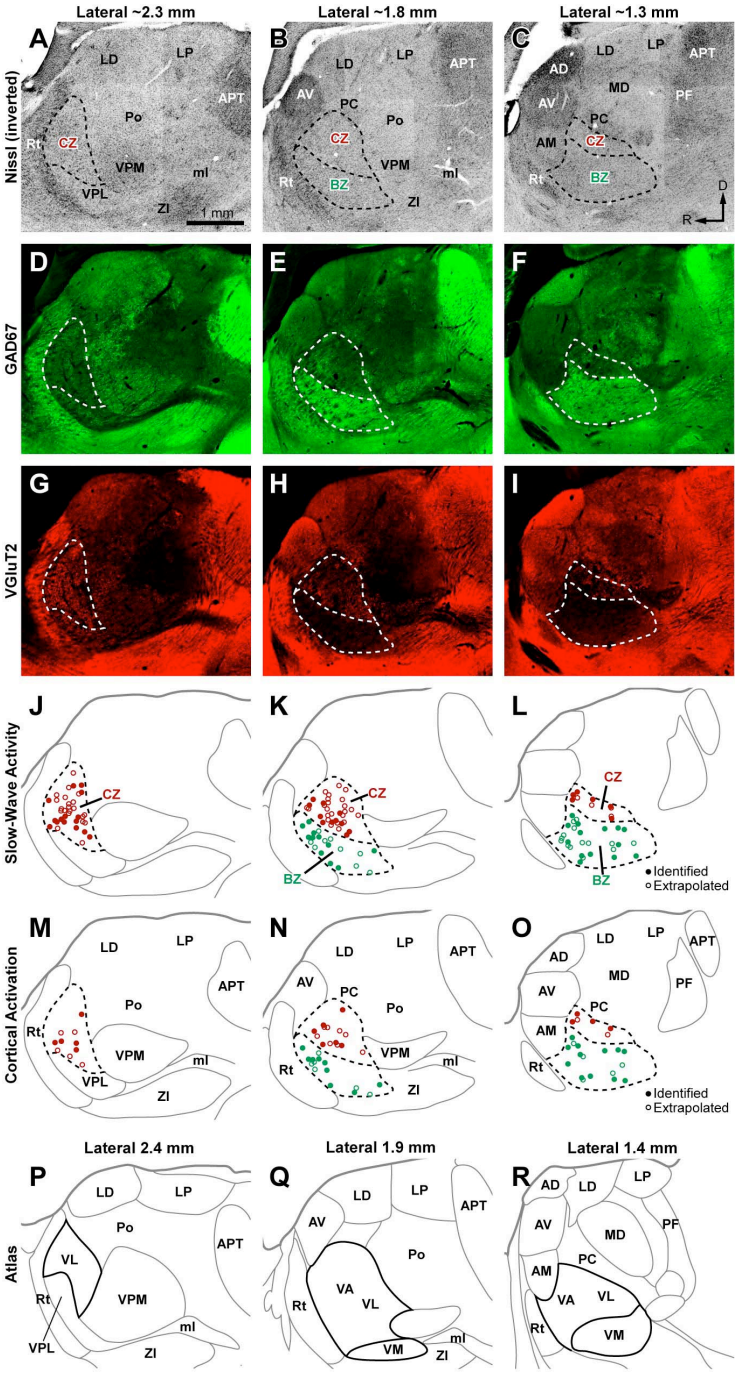

Supplementary Figure 2. Localization of all recorded thalamic neurons to immunohistochemically-defined input zones. (*A–I*) Parasagittal views of the rat motor thalamus at three different mediolateral planes; ~2.3 mm (*A, D, G*), ~1.8 mm (*B, E, H*), and ~1.3 mm (*C, F, I*) lateral to Bregma. To delineate the basal ganglia-recipient zone (BZ) and cerebellar-recipient zone (CZ) of the motor thalamus (borders indicated by dashed lines), tissue sections were triple fluorescently labeled for Nissl substance (inverted tone;

A–C), GAD67 (*D–F*), and VGluT2 (*G–I*); fluorescence images of the three markers are presented separately here. (*J–O*) Locations of the identified and extrapolated neurons recorded during either SWA (*J–L*) or cortical activation (*M–O*), as plotted at the same parasagittal planes as above. Borders between nuclei in *J–O* were omitted when they could not be unambiguously delineated with labeling for Nissl substance, GAD67 or VGluT2. (*P–R*) Delineation of thalamic nuclei according to the closest three parasagittal planes available (lateral from Bregma: 2.4, 1.9 and 1.4 mm) in a widely-used rat brain atlas (Paxinos and Watson 2007). Note that the boundaries of BZ and CZ (dashed lines) do not match nuclear borders delineated in the atlas on cytoarchitectonic grounds (solid lines). Abbreviations are defined in Figures 1 and 2. Scale bar in *A* also applies to all other panels.

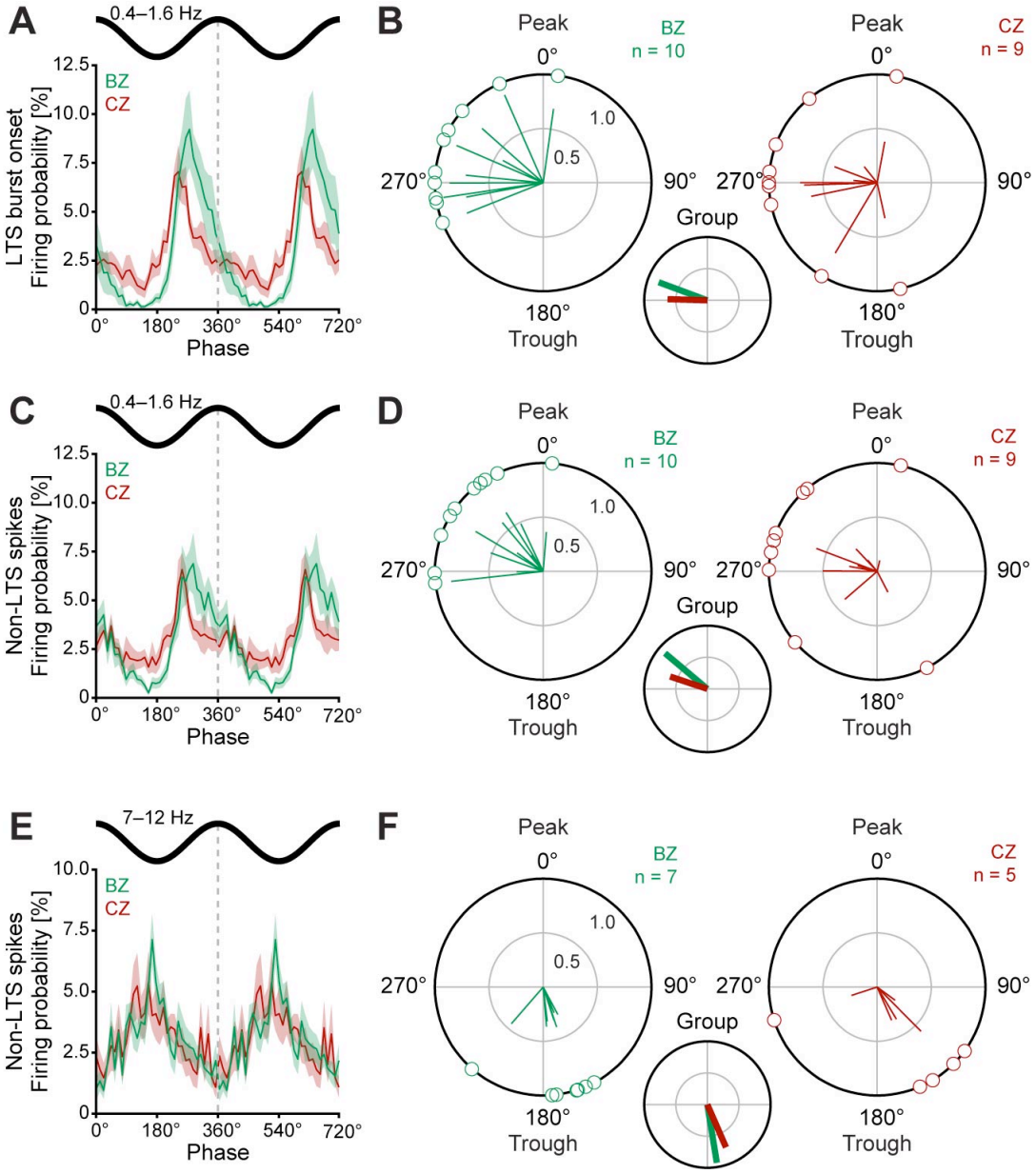

Supplementary Figure 3. Timings of non-LTS spikes of neurons in the basal ganglia-recipient and cerebellar-recipient zones in relation to cortical slow oscillations (0.4–1.6 Hz) and spindle oscillations (7–12 Hz). Analyses of non-LTS spikes, *i.e.* those not contained within defined LTS bursts, were carried out on a subset of thalamic neurons that fired >60 such spikes. (*A*) Linear phase histograms of the first spike in each LTS burst for neurons in the basal ganglia-recipient zone (BZ; $n = 10$, green) and neurons in the cerebellar-recipient zone (CZ; $n = 10$, red). For clarity, two cortical oscillation cycles are shown. (*B*) Circular plots of phase-locked firing of qualifying BZ neurons (green) and CZ neurons (red). Vectors of preferred firing of individual neurons are shown as lines radiating from the center. Greater vector lengths indicate lower variance in the distribution around the mean

phase angle. Each circle on the plot perimeter represents the preferred phase (*i.e.* mean phase of all the spikes) of an individual neuron. A mean vector for preferred phases of neurons in each group is shown as a thick line (BZ in green, CZ in red) in the smaller circular plot. (*C, D*) As in *A* and *B*, but for the non-LTS spikes of the same neurons. (*E, F*) As in *C* and *D*, but for spindle oscillations. Only neurons that were significantly phase-locked ($P < 0.05$, Rayleigh's Uniformity Tests) were included in *B*, *D* and *F*. Data in *A*, *C* and *E* are means ± SEMs. *n*, the number of neurons analyzed.

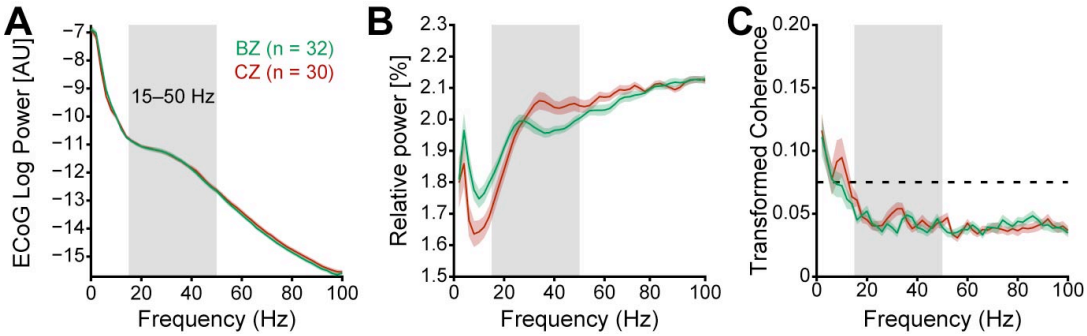

Supplementary Figure 4. Spectral analyses of ECoGs, thalamic neuron spike discharges, and their coherence during cortical activation. (*A*) Mean power spectra of ECoGs simultaneously recorded with all neurons in the basal ganglia-recipient zone (BZ; green) or with all neurons in the cerebellar-recipient zone (CZ; red). (*B*) Mean power spectra of the spike discharges of BZ neurons (green) and CZ neurons (red) relative to power at 0–100 Hz. (*C*) Mean coherence spectra between ECoGs and all BZ neurons (green) or all CZ neurons (red). The dashed horizontal line denotes the 95% confidence level. Gray boxes in *A–C* indicate the frequency range of oscillations analyzed (15–50 Hz). Data are mean ± SEMs. *n*, the number of neurons/ECoGs analyzed.